Numerical Model Sensitivity to Heterogeneous Satellite Derived Vegetation Roughness

Michael Jasinski
Hydrological Sciences Branch, NASA Goddard Space Flight center, Greenbelt, MD

Joseph Eastman
WindLogics Inc., Grand Rapids, MN

Jordan Borak
Wyle Information Systems, LLC, Greenbelt, MD

Agricultural and Forest Meteorology
April 2011

Corresponding author address: Michael Jasinski, Hydrological Sciences Branch, Code 614.3, NASA Goddard Space Flight Center, Greenbelt, MD 20771
E-mail: Michael.Jasinski@nasa.gov

Abstract

The sensitivity of a mesoscale weather prediction model to a 1 km satellite-based vegetation roughness initialization is investigated for a domain within the south central United States. Three different roughness databases are employed: i) a control or standard lookup table roughness that is a function only of land cover type, ii) a spatially heterogeneous roughness database, specific to the domain, that was previously derived using a physically based procedure and Moderate Resolution Imaging Spectroradiometer (MODIS) imagery, and iii) a MODIS climatologic roughness database that like (i) is a function only of land cover type, but possesses domain specific mean values from (ii). The model used is the Weather Research and Forecast Model (WRF) coupled to the Community Land Model within the Land Information System (LIS). For each simulation, a statistical comparison is made between modeled results and ground observations within a domain including Oklahoma, Eastern Arkansas, and Northwest Louisiana during a 4-day period within IHOP 2002. Sensitivity analysis compares the impact the three roughness initializations on time-series temperature, precipitation probability of detection (POD), average wind speed, boundary layer height, and turbulent kinetic energy (TKE). Overall, the results indicate that, for the current investigation, replacement of the standard look-up table values with the satellite-derived values statistically improves model performance for most observed variables. Such natural roughness heterogeneity enhances the surface wind speed, PBL height and TKE production up to 10 percent, with a lesser effect over grassland, and greater effect over mixed land cover domains.

1. Introduction

Nearly all land surface hydrology, weather forecast, and global circulation models used today rely on some form of Monin-Obukhov similarity theory for estimating surface momentum and other scalar fluxes such as sensible and latent heat. For momentum, the similarity equation is,

$$\frac{\mathrm{u}(z)}{u_*} = \frac{1}{\kappa}\left[\ln\left(\frac{z-d_0}{z_0}\right) - \Psi(\varsigma)\right], \quad (1)$$

where u(z) is the mean surface layer wind speed at height z, u_* is the friction velocity, κ is von Karman's constant, and $\Psi(\zeta)$ is the adjustment function due to stability. The two roughness parameters are z_0, the roughness length for momentum, and d_0, the zero plane displacement height, an elevation adjustment to the wind profile in the presence of vegetation. The formulation parameterizes the decrease in wind speed due to increases in either z_0 or d_0, with the influence of d_0 decreasing with height. Analogous similarity expressions are used for the sensible and latent heat fluxes in terms of z_{0h} and z_{0v}, the roughness lengths for sensible heat and water vapor, respectively.

a. Difficulties in evaluating roughness

Although simple conceptually, z_0 and d_0 are not easily modeled and cannot be directly measured. They are best determined from analysis of flux-profile measurements taken during field experiments at near-neutral atmospheric conditions (e.g. Brutsaert 1982). Because of this large effort, obtaining in situ estimates for every grid box in a numerical

model is prohibitive. Consequently, the typical practice is to simply assign monthly or seasonal z_0 and d_0 values based solely on land cover type using look-up tables. Table 1 displays values from several sources including field experiments (Brutsaert, 1982), values assumed proportional to land cover height such as those employed in the Community Land Model (CLM2) (Bonan et al. 2002), values derived from climatology and phenology of various land cover types such as the NOAH Land Surface Scheme (Dorman and Sellers 1989) and the Biosphere Atmosphere Transfer Scheme (BATS) (Dickinson et al. 1993). Also included are the mean MODIS based values derived in this study specifically for the south central U.S.

The table illustrates limitations to the look-up table approach. First, there is no clear consensus for a given land cover type. For example, mean values range from 0.8 to 1.5, 0.4 to 1.1, and 0.56 to 1.1 for evergreen needleleaf, deciduous broadleaf and mixed forests, respectively. Second, it can not adequately accommodate spatial and temporal heterogeneity, especially when study areas cover long integration periods and large spatial domains. Models are thus inflexible to canopy density, seasonal growth and senescence, and within class variability. For example, data from Eagleson (2000; Fig 4.15, p. 107) show that for fourteen different forest stands all classified as evergreen needleleaf, the mean z_0 was 1.44 m with nearly an equal standard deviation of 1.45 m. Mean d_0 was 14.2m with 6.4m standard deviation. Data from Brutsaert (2006) indicate short grass roughness ranges from 0.008 to 0.02m, while long grass roughness ranges from 0.02 to 0.06 m. Driese and Reiners (1997) reported shrubland roughness from 0.01 to 0.07m.

Clearly, the implication is that a single roughness value does not represent all plant canopies within a land cover type.

In order to more easily characterize spatially variable roughness, remote sensing approaches have been developed. Several extend previously developed surface roughness parameterizations (e.g. Raupach 1994; Massman 1997; Lindroth 1993) to the scale of the pixel, with satellite data providing a measure of canopy density in the form of fractional cover or leaf area. They include geometric modeling of the Landes forest, France using Landsat imagery (Jasinski and Crago 1999), investigations of the Canadian boreal forest using aircraft meteorology observations (Yang and Friedl 2002) and AVHRR imagery (Schaudt and Dickinson 2000), MODIS-based investigations over the south central United States (Jasinski et al. 2005; Borak et al. 2005). Empirical associations with SRTM and JERS-1 imagery also have been presented (Saatchi et al. 2001). Additional physical models suitable for satellite applications also have been developed (Zilintikevitch et al. 2008; Nakia et al. 2008; Zhong et al. 2007; Lu et al. 2009).

b. Importance of roughness variability

Numerous investigators have suggested the importance of the roughness parameterization to land surface fluxes (e.g. Crago 1998; Zhang and Anthes 1982; Zhao and Pitman 2002). Such studies indicate that for changes in roughness length by about 25%, there is a corresponding change in latent or sensible heat fluxes by 3 to 5%.

Roughness has been investigated within the context of land cover change and deforestation (e.g., Hahmann and Dickinson 1997; Lean and Rowntree 1997; Sud and Smith 1985; Sud et al. 1996). Reduced roughness length generally decreases the turbulent energy fluxes, which tends to increase temperature (Sellers 1992; Zhang et al. 1996). Dickinson & Henderson-Sellers (1988) concluded that decreased roughness due to replacement of tropical forests with grassland leads to decreased sensible and latent heat fluxes and increased vegetation and soil temperatures. Sud et al. (1988) found only small changes in sensible and latent heat fluxes, but large variations in boundary layer wind speed and atmospheric circulation and rainfall distribution, particularly along coasts where large roughness discontinuities occur. Abiodun et al (2008) determined that the simulated increase in monsoon flow can be attributed to the reduction in surface roughness from deforestation.

The impact of roughness heterogeneity has been studied using both coupled land-atmosphere and uncoupled land models. Early investigations indicated that mesoscale roughness heterogeneity had a small effect on larger domain averaged fluxes (Zhong and Doran, 1998), although heterogeneity in land use patterns over Oklahoma was shown to affect land-air interactions (Weaver and Avissar, 2001). More recently, Bou-Zeid et al. 2007 developed a parameterization between blending height and heterogeneous roughness using a Large-Eddy Simulation (LES) model. Courault et al. 2007, also using an LES model, determined that surface fluxes can vary by about 5 percent depending on the arrangement of the surface cover patches. However, Huang et al. 2008 showed little sensitivity in scalar fluxes to different hypothetical land surface representations. Milly

and Smakin (2002) concluded that surface roughness variability had little impact on uncoupled, global energy and water balance models. However, large-scale coupled GCMs have shown otherwise. Hahmann and Dickinson (2001) found that horizontal heterogeneities in surface roughness and albedo affect precipitation over tropical land. Zeng and Wang's (2007) formulation, focusing on the convergence of roughness at low canopy densities, resulted in improved sensible and latent heat fluxes when compared to the Cabauw data set. Klink (1992) also showed that sub-GCM grid scale canopy discontinuities were important.

Several recent studies have focused on surface heterogeneities the U.S. Southern Great Plains. Weaver (2004) concluded, using high resolution modeling, that the relative influence of surface heterogeneity depends on synoptic scale meteorology. During dry periods and periods characterized by large-scale mean subsidence, surface heterogeneity enhances vertical motion and mesoscale fluxes that in turn affect domain averaged dynamics. Using aircraft observations during IHOP 2002, Kang et al. (2007) also concluded that small-scale surface moisture and temperature heterogeneities can affect boundary layer development. However, Kang and Davis (2008) doubted the ability of mesoscale models to properly account for such heterogeneities in simulating the atmospheric boundary layer.

2. Satellite-Based Vegetation Momentum Roughness

a. Roughness formulation

The approach used to generate the roughness datasets in this study was previously described in Jasinski et al. (2005) and Borak et al. (2005). It utilizes Raupach's (1994) roughness formulation for surface stress partition that assumes drag elements superposed on a flat surface, but with two modifications. First, instead of using a single set of drag parameters that represents all land cover types, it employs a separate set of parameters derived for each major classification within the International Geosphere-Biosphere Programme (IGBP). Second, it develops estimates of canopy area index on a pixel by pixel basis using a combination of satellite-based leaf area and a seasonally varying stem area. The two extensions to Raupach's original formulation lead to estimates for z_0 and d_0 at the scale the satellite pixel or model grid box.

The momentum roughness length is expressed following Raupach (1994,1995) or,

$$\frac{z_0}{h} = \left(1 - \frac{d_0}{h}\right) \exp\left(-\kappa \frac{U_h}{u_*} + \psi_h\right), \quad (2)$$

where h is element height, and U_h and ψ_h are the wind speed and the roughness sublayer influence function, respectively, at height h. The ratio U_h / u_* is expressed

$$\frac{U_h}{u_*} = \gamma = \left(C_S + \frac{\Lambda C_R}{2}\right)^{-1/2} \exp\left(\frac{c\Lambda\gamma}{4}\right), \quad (3)$$

where C_S is the drag coefficient of the substrate, C_R is the drag coefficient of the individual roughness elements, and c is a sheltering coefficient. The canopy area index, Λ, further described below, is defined as the total single sided area of all momentum absorbing elements per unit ground area. As Λ increases to Λ_{max}, flow starts to skim over the canopy rather than pass through it. At this point and for all greater canopy densities, the ratio $\frac{u_*}{U_h}$ attains a constant value or,

$$\frac{u_*}{U_h} = \left(\frac{u_*}{U_h}\right)_{\max} = \gamma_{\max}^{-1} \qquad \text{for all } \Lambda > \Lambda_{max} \quad . (4)$$

The zero-plane displacement is similar to Raupach's expression but rewritten as,

$$\frac{d_0}{h} = \left(\frac{\beta\Lambda}{2+\beta\Lambda}\right)\left[1-\alpha\gamma^{-1}\Lambda^{-1/2}\right] \quad (5)$$

,

where β represents the ratio C_R/C_S and α is an empirical constant.

Equations (2) through (5) are used to develop plots of d_0/h vs. Λ and z_0/h vs. Λ. The parameters C_R, α, c, γ_{max}, and Λ_{max} , required for each land cover type and shown in Table 2, were previously reported in Jasinski et al. (2005) using the Method of Moments and published roughnesses from the literature and various field experiments. Typical plots for two cover types, evergreen needleleaf and grassland, are shown in Figure 1 below. The plots are the basis for constructing the roughness fields when Λ is determined from satellite imagery.

b. MODIS based Canopy Area Index and roughness fields

The single variable in the formulation is Λ. It is approximately equal to the sum of the green canopy matter per unit vegetated area, L_{gv}, and the stem and dead area matter per unit vegetated area, L_s, or

$$\Lambda \sim L_{gv} + L_s. \quad (6)$$

Since dead matter is a function of prior canopy states, the non-green term of canopy area index is written as a time-varying component or

$$L_s^n = \max\left\{\left[aL_s^{n-1} + \max(L_{gv}^{n-1} - L_{gv}^n, 0)\right], L_{s,\min}\right\}, \quad (7)$$

where *n* represents time period, (1- *a*) and $L_{s,\min}$ are the removal rate of dead leaves and the minimum estimated value for L_s, respectively, for the land cover type associated with the pixel of interest (see Zeng et al., 2002 and Borak et al. (2005)). In the current study, *n* and *n* – 1 are the MODIS 8-day compositing periods for June 2-9, 2002, and May 25-June 1, 2002, respectively. Equations (6) and (7) are thus used to estimate Λ for each pixel in the domain covering south central United States, as shown in Figure 2.

Applying Figure 2 to the extended Raupach formulation yields a spatial time series of z_0 and d_0 fields for the MODIS June 2-9, 2002 compositing period, shown in Figures 3a and 3b, respectively. The new satellite-derived fields exhibit significant spatial and temporal variability, with an overall gradient of increasing roughness from northwest to southeast as vegetation changes from grassland to mixed forest. Since the original formulation yields normalized roughnesses, fields of absolute roughness have been computed by multiplying the results by climatological heights (Dorman and Sellers 1987). Global grid-based canopy heights are not currently available. However, within

the next decade, new satellite altimeters such as DESDynI and ICESat-II should provide more spatially detailed canopy height data.

3. Coupled Mesoscale Simulation Model

a. Model description and setup

The modeling system used is the Weather Research and Forecast (WRF-ARW), (Skamarock et al 2005) model coupled to the Community Land Model version 2.0 (CLM2) embedded in the Land Information System (LIS), (Kumar et al. 2004). The fully integrated system or LISWRF, was facilitated by the structure and tools provided by the Earth System Modeling Framework. Satellite derived roughness fields were incorporated into LISWRF through modifications within LIS.

The principal WRF modeling options included the Rapid Radiative Transfer Model (RRTM) longwave scheme (Mlawer et al. 1997), the Goddard shortwave scheme (Chou and Suarez 1994), and the Ferrier (Lin et al. 1983) and Rutledge and Hobbs (1984) microphysics. The radiative transfer in RRTM is performed using the correlated-k method with the k distributions attained directly from Line By Line Radiative Transfer Model (LBLRTM). The Mellor-Yamada-Janjic (MYJ) surface layer scheme (Janjic 2002) is employed. Over water surfaces the viscous sublayer is parameterized explicitly following Janjic (1994). Over land, the effects of the viscous sublayer are taken into account through variable roughness height for temperature and humidity as proposed by Zilitinkevitch (1995). The Beljaars (1994) correction is applied in order to avoid singularities in the case of an unstable surface layer and vanishing wind speed. In this implementation, an upper limit is imposed on the master length scale. This upper limit

depends on turbulent kinetic energy (TKE) and the buoyancy and shear of the driving flow. In the unstable range the functional form of the upper limit is derived from the requirement that the TKE production be nonsingular in the case of growing turbulence. In the stable range the upper limit is derived from the requirement that the ratio of the variance of the vertical velocity deviation and TKE cannot be smaller than that corresponding to the regime of vanishing turbulence. The TKE production/dissipation differential equation is also solved iteratively.

b. Domain characteristics

The full model domain or FULL is shown in Figure 4 together with the land cover classification scheme. It was chosen to cover both grassland and forested classes, and extends over much of Oklahoma, Arkansas, northeastern Texas and northwestern Louisiana. The grid consists of 810x710 horizontal points at 1km spacing and 46 vertical levels, stretched from 17m spacing at the surface to 1km at the model top. Within FULL, two subdomains of the same size but with different dominant land covers classes are identified. GRASS, located in the northwestern quadrant of FULL entirely in Oklahoma, is dominated by IGBP classes Grassland and Cropland. MIXED is located in the opposite southeastern quadrant of FULL in northeastern Louisiana. MIXED is dominated by Mixed and Deciduous Broadleaf Forests, and Woody Savanna, although about half the area in non-forest. Both the GRASS and MIXED subdomains are characterized by flat to low relief.

A case period was chosen, starting at 12GMT on June 3, 2002 and ending at 12GMT on June 7, 2002, that represented a variety of synoptic conditions. The first 60 hours of the

period were dominated by a frontal passage and associated convection. The last 36 hours were characterized by a dry-down period with relatively light synoptic forcing.

The initial meteorological fields were assimilated from the North American Regional Reanalysis (NARR, http://wwwt.emc.ncep.noaa.gov/mmb/rreanl/index.html) gridded data, which also provided nudged boundary conditions on the lateral boundaries of the domain at three hour resolution. The NARR 32km horizontal mesh data were ingested into the WRF Standard Initialization (WRFSI) system using a 16-point interpolation method.

The soil thermodynamic profiles were initialized by a 2.5 year offline integration of LIS using observed forcing data and roughness values set according to the default CLM2 look-up table. The LIS model employed meteorological forcing from the North American Land Data Assimilation System (NLDAS, Mitchell et al. 2004) in conjunction with soil data derived the State Soil Geographic (STATSGO, Soil Survey Staff, Natural Resources Conservation Service, United States Department of Agriculture) database. Finally, vegetation was initialized using the Version 4 MODIS Land Cover Product, IGBP data layer (Friedl et al. 2002).

c. Roughness cases

Three integrations were performed with the only difference being the z_0 and d_0 initialization fields. The default or control case, CONTR, utilizes the standard or universal lookup table roughnesses based solely on CLM2 land class as shown in Tables 3a and 3b. For the second simulation or HETER, each 1 km LISWRF grid box was assigned unique MODIS-derived z_0 and d_0 associated with June 3-7, 2002 satellite

observations as described in Section 2 and Figures 3a and 3b. The third case, CLIMO, assumes constant z_0 and d_0 for each land cover type, equal to the mean of the HETER FULL domain. CLIMO is thus similar to CONTR in that it is essentially a look-up table approach, but with mean MODIS values.

A summary of the MODIS-derived mean and standard deviation of z_0 and d_0 for each land cover type within the GRASS, MIXED and FULL domains are provided in Tables 3a and 3b, respectively. The three largest cover types in GRASS are Grassland, Cropland Vegetation Mosaic, and Cropland that occupy 61.5%, 18.8% and 11.2% of the subdomain, respectively. Mean z_0 (d_0) for the same three cover types are 0.07 (0.35), 0.05 (0.27), and 0.04 (0.25), respectively. Standard deviations are very low, about 15% to 20% of mean values. The MODIS z_0 and d_0 values are lower than the CLM values 0.06 (0.34), but closer to the mean of nine IHOP field sites reported in the 10-day period surrounding the current investigation or 0.03 (0.15) (Horst, 2002). When averaged over all land covers in GRASS, however, mean z_0 for HETER and CLIMO are the same as CONTR.

For the MIXED subdomain, the principal land cover types are Woody Savanna, Mixed Forest, and Deciduous Broadleaf Forest, covering 22.4%, 19.6%, and 14.7%, respectively, with other cover types more evenly distributed. Mean z_0 (d_0) are 0.90 (2.58), 0.64 (6.21), and 0.61 (5.63), respectively. Standard deviations are much higher for MIXED, especially for forested areas, where values are about the same order of magnitude as the mean. Overall, values are lower than CLM roughness, but within the range reported by Brutsaert (1984) and also somewhat closer to those reported by Dorman and Sellers (1989) and

Dickinson et al. (1993) in Table 1. Similar conclusions can be made for the FULL domain average.

4. Results

a. Quantification of model error

A statistical comparison was conducted between the simulated fields and available ground station observations. Observations included i) roughly 250 surface meteorological stations dispersed throughout the domain that measure surface pressure (PSFC), temperature at 2 meters (T2), dew point temperature (TD), and wind speed (WSPD) and direction, ii) eight flux stations from the Oklahoma Mesonet (Brock et al, 1995) that included net longwave radiation (LWD), net shortwave radiation (SWD), sensitive heat (H) and latent heat (LH), and iii) the NCEP Stage IV 4km gridded precipitation data.

Three statistics were used to compare modeled and observed values. The model bias was defined as,

$$\mathrm{BIAS} = \frac{1}{N}\sum_{i=1}^{N}\left(\mathrm{Mod}_i - \mathrm{Obs}_i\right),$$

where Obs_i is the ground truth observation, Mod_i is the LISWRF estimate using an inverse-squared distance weighting from the station to the nearest four model grid boxes, and N is the number of evaluations within a given time-step. Evaluation at the meteorological stations was performed at hourly intervals. Short and longwave radiation, latent heat, and sensible heat fluxes were evaluated at 15 minute intervals. NCEP precipitation data were evaluated at hourly intervals.

Root mean square error was defined

$$\mathrm{RMSE} = \left[\frac{1}{N} \sum_{i=1}^{N} \left(\mathrm{Mod}_i - \mathrm{Obs}_i \right)^2 \right]^{1/2},$$

and mean absolute error was defined

$$\mathrm{MAE} = \frac{1}{N} \sum_{i=1}^{N} \left| \mathrm{Mod}_i - \mathrm{Obs}_i \right|,$$

Results for the FULL domain are displayed in Table 4 for HETER, CLIMO, and CONTR integrations for meteorological quantities and surface fluxes. Tables 5 and 6 show the results for the GRASS and MIXED subdomains, respectively. The lowest values for each variable and statistic are indicated by bold underline. For the FULL domain, results indicate that the HETER integration had the lowest error in 15 of 24 statistics. Of particular interest was a large reduction in the temperature BIAS of over 0.5 degrees. For the GRASS subdomain, seven of 12 lowest error statistics occurred in the HETER case, with the remaining in the CLIMO case, and none in CONTR. For the MIXED subdomain, ten of twelve error statistics were lowest in the HETER and CLIMO cases, with most occurring in CLIMO and only two in CONTR. The results thus indicate that, for this study, the satellite derived roughness fields reduce overall model error. Further, it is observed that for most variables, the statistics of CLIMO and CONTR agree more closely than those from HETER. This is especially true for BIAS.

Also examined was the time series diurnal behavior of the temperature BIAS. This is displayed in Figure 5, for HETER (solid line), CLIMO (short dashes), and CONTR (long

dashes). Throughout the 96 hours of the simulations the HETER consistently exhibits the least cool BIAS during the daytime hours but seems to have a slightly higher warm BIAS at night. The higher warm BIAS at night could be due to higher ground temperatures produced during the day and an underestimate of outgoing longwave radiation. The cool daytime BIAS and warm night time BIAS of CLM is a known weakness of this particular land surface scheme (Zeng et al. 2002).

Figure 6 displays domain-averaged probability of detection (POD) of precipitation for the three different simulations over the 96 hour period. A threshold of 2.54mm was used when evaluating POD. A POD of 1 would be a perfect forecast. The bulk of precipitation occurs between 14GMT on June 4, 2002 and 20GMT on June 5, 2002. The precipitation is forced by a frontal passage and initially the models exhibit similar skill. The HETER integration shows a slightly higher POD both initially and when averaged over time. Although the POD seems rather small for all the integrations, these values are similar to what Weisman et al. (2008) found using WRF over the central US at similar model resolutions. It is interesting to note that around hour 84 of the integration, there was some popcorn precipitation in the southeast HETER portion of the domain. HETER actually indicates a small POD a few hours before the other integrations. During this time period synoptic forcing was quite weak. It is possible that the heterogeneity in the aerodynamic parameters alters the low level moisture flux convergence in such a way as to trigger the convection. It was pointed out in Lin and Glendening (2002) that discontinuities in surface roughness lead to the formation of an internal boundary layer (IBL). The heterogeneous surface roughness in HETER would also lead to a complex pattern of IBLs and contribute to instabilities at some locations further contributing to shallow convection.

b. Model sensitivity to satellite-based roughness

The sensitivity of LISWRF to the three roughness initializations was examined by comparing time series domain averages to selected output. Figure 7a displays the domain averaged wind speed at 2m for the 3 integrations for the FULL domain over the 96 hour integration period. The differences appear quite small over the time interval, although there is a tendency toward higher wind speeds during daytime hours in the HETER simulation. This might be expected since the mean roughness for HETER was slightly less than for CONTR. However, the effect does not occur for CLIMO that also possesses the same mean as HETER. The figure also shows how the wind speeds decreased throughout the simulation as the cool front moved through the domain.

Figure 7b displays the time series differences in domain averaged wind speeds with the differences in the HETER and CLIMO runs (HETER-CLIMO) plotted as a solid line, HETER-CONTR as a dashed line, and CLIMO-CONTR as a dotted line. This figure clearly shows the influence of roughness heterogeneity, with nearly zero difference at all times between the CLIMO and CONTR simulations that contain no within class variability. To the contrary, the differences for HETER – CLIMO and HETER - CONTR are substantially higher on the order of about 0.3 m/s, or about 5% during the daytime.

Figures 8a-b are similar to Figures 7a-b except that it applies to GRASS, the domain with the smallest magnitudes in roughness. The figures indicate mixed results, although differences with HETER are generally greatest. The high frequency fluctuations in the middle of the integrations are due to the initiation of fairly intense convection and

subsequent development of gust fronts, and these highly non-linear events lead to the largest fluctuations in differences between CLIMO and CONTR.

Figure 9a-b displays the domain averaged wind speed and differences for the MIXED domain, respectively. Here, the differences between HETER- CONTR and HETER-CLIMO were significant during the day. Figure 9b exhibits the clearest example of the impact of heterogeneity, with any significant differences in CLIMO and CONTR only occurring during weak convective events. The figure also indicates that when the roughness variability is high, as in the MIXED domain, the effect on domain averaged wind speed can be over 10 percent of its magnitude during the daytime hours.

In order to examine the vertical extent of the surface roughness heterogeneity, a similar comparison was made for the simulated planetary boundary layer (PBL) heights. For the FULL domain, Figure 10a displays the domain averaged PBL heights while Figure 10b displays height differences. The results from HETER-CLIMO and HETER-CONTR show that the PBL height is consistently enhanced when roughness heterogeneity is present. This enhancement ranges to about 5% for the current study. One possible explanation is that the daytime wind speed increase found in the previous plots leads to an increase in TKE shear production which is in turn communicated up through boundary layer eddies which also could be further magnified by the drag effect due to roughness heterogeneity. Examination of similar PBL plots for the GRASS and MIXED subdomains, displayed in Figures 11a-b and 12a-b, respectively, follow the same trend found in the plots of wind. GRASS plots indicates only slight differences, while MIXED plots exhibit much larger PBL differences of 10% or more.

In addition to the enhanced PBL height for the HETER case, perhaps an equally interesting feature is that growth and decay rates are also increased, with the collapse of the PBL being the most evident. One predominant characteristic of mesoscale models is their difficulty in properly simulating accurate PBL dynamics including the rapid collapse of the PBL (Angevine and Mitchell, 2001). This would also be of importance to transport and dispersion modeling in both horizontal and vertical directions. As wind advects from smaller to higher roughnesses, convergence will result enhancing vertical motion. Similarly, when advecting from higher to smaller roughnesses, divergence will result and tend to decrease vertical motion. The altering of vertical motion is occurring to some degree at all grid cells within the domain, with the net effect causing a broadening of the vertical velocity spectrum and a reduction in the areas with near zero values. In the MIXED subdomain, there is considerably more variance in roughness and there should be a larger effect than the GRASS counterpart.

In order to examine the drag effect on the vertical motion, an empirical probability distribution function (PDF) was computed of the domain averaged vertical motion for each hour over the 4 day period. Shown in Figure 13 are the PDF's for all integrations of the 4 day average for 20GMT at 726m above ground level. The vertical velocity bins were calculated at 0.01m/s intervals. The bins were truncated with values less than -2.0 m/s and higher than 2.0 m/s so that effect of variable roughness can be seen more clearly. The figure indicates that CLIMO (dashed line) and CONTR (dotted line) have a remarkably similar distribution, while HETER (solid line) exhibits a broadening of the right and left hand tails. Further, HETER exhibits an approximately 25% reduction in the near zero values as compared to both the CLIMO and CONTR cases.

Figures 14 and 15 were calculated over the GRASS, and MIXED subdomains, respectively. The PDFs for all three integrations are quite similar for GRASS although there is a reduction of 15% in the near zero values. Examination of MIXED shows, for the HETER simulation, pronounced reduction in the near zero vertical motion of about 30-35%, and broadening of the spectrum as compared to CLIMO and CONTR. In a separate analysis of kurtosis it was found that the HETER integration exhibits lower values for nearly all times and levels throughout the PBL and in the nocturnal boundary layer, indicating a broadening of distribution.

The impact to vertical motion also was examined with respect to TKE production. Figure 16 shows the TKE profile, domain averaged over FULL, and temporally averaged over the 4 day simulation at 18GMT. Overall, the figure exhibits a comparative increase in TKE for HETER of 5 to 10 percent up to model level 15, which is approximately 1655m above the ground. The second level, at about 40 m, exhibits the largest difference for HETER or about 10 percent, compared to CONTR and CLIMO which are almost indistinguishable. Results for the GRASS and MIXED domains are shown in Figures 17 and 18, respectively. GRASS experiences daytime differences of up to about 5 percent when heterogeneity is present, with a maximum at the second level. For the MIXED region, HETER show consistently higher TKE over almost all levels compared to CONTR and CLIMO. The difference is largest at the second model level near the top of the surface layer, at about 8%.

Finally, Figures 19, 20 and 21 expand on the above plots, by showing the four-day time series, domain averaged TKE at the second level for FULL, GRASS and MIXED

domains, respectively. The impact of the heterogeneity is evident through all domains, with about a 10% or larger increase in TKE near mid-day, and the trend reversed after the collapse of the boundary layer and onset of the nocturnal boundary layer. GRASS shows the least effect throughout the integration.

In Lin and Glendening (2002), the authors use an LES model, with 10m horizontal grid spacing, to resolve the generation of an internal boundary layer when flow moves from a smooth to a rough surface, or vice versa. They found that there was an induced pressure gradient above the surface layer that tends to accelerate the flow over a rough surface, or decelerate over a smooth surface. In the surface layer there is will be a deceleration over the rough surface, that when it is coupled with the opposite behavior above the surface layer should tend to generate more TKE through the shear production term for TKE. One would also expect the pressure and turbulent transfer terms of the TKE budget to be enhanced due to the added perturbation due to heterogeneity. Finally, temperatures from the present simulation were roughly 0.7C higher in the HETER case, implying increased TKE generation through the buoyancy term.

5. Summary

A procedure for developing realistic, domain specific roughness heterogeneity for use within a numerical weather prediction model has been presented using satellite imagery combined with a physical model of surface stress partition. In the current study, the 1 km resolution MODIS Leaf Area Index and Land Cover Type Data Products are used to compute Canopy Area Index on a pixel by pixel basis. They in turn are used with land cover specific drag parameters within Raupach's formulation to estimate a unique z_0

and d_0 for each 1 km grid box in the simulation domain for the June 3-7 2002 period. While not intended as a substitute for *in situ* observations of z_0 and d_0, the approach provides spatially heterogeneous roughness fields that are more realistic, both spatially and temporally, than the current look-up table approach. While the current study employed MODIS LAI, the procedure to derive roughness can employ any gridded LAI data product, including Landsat ETM and NOAA AVHRR, as long as the necessary fetch and footprint scales associated with the determination of roughness are respected.

Mean MODIS based roughnesses computed for the GRASS subdomain were about the same as CLM default roughnesses. However, for MIXED and FULL they were about 20% lower. Roughness standard deviations per cover type ranged from about 10% of the mean in Grassland and other non-foreseted cover types up to 100% in some forested regions.

The impacts of the MODIS fields within LISWRF were manifested in several ways. First, simulations with MODIS-based HETER and CLIMO roughness fields yielded overall statistically improved results over CONTR when compared with available observations, especially in regions of high roughness variability. Comparison of the HETER-CLIMO, HETER-CONTR, and CLIMO-CONTR difference plots indicates, however, that the impact of the heterogeneity is much greater than the impact due to the ~20% difference between mean MODIS and CLM roughnesses. Impacts were small in the GRASS subdomain. Difference plots indicate for the current study that the impact of roughness heterogeneity on wind and PBL height was about 5 % for FULL, 10% for

MIXED, and only a few percent for GRASS, depending on time of day. The impact on TKE was about 10% for FULL, 10-20% for MIXED, and several percent for GRASS. During periods of strong convection, the impact of roughness heterogeneity is not conclusive. These results are thus consistent with earlier reporting by Sellers (1992), Zhang et al. (1996), Weaver (2004) and Courault et al. (2007).

The above results were obtained with simulations conducted at the same resolution. This leads one to conclude that, at least for the domain and time period studied, increases in natural roughness heterogeneity induces increases in LISWRF modeled wind speed, PBL height, and TKE production. The detail of the roughness fields is commensurate with the level of detail in today's higher resolution mesoscale models. Additional testing is warranted. Future work may include repeating the simulations at different grid box scales, extending the modeling efforts over different seasons and locations, and examining the impact of roughness heterogeneity on surface fluxes.

Acknowledgments. Research was supported by NASA's Applied Sciences Homeland Security and Disaster Management Programs, and the Terrestrial Hydrology Program.

References

Abiodun, B., S. Pal, E. Afiesimama, W. Gutowski, and A. Adedoyin, 2008: Simulation of West African monsoon using RegCM3 Part II: impacts of deforestation and desertification *Theor. Appl. Climatol*. **93**, 245–261.

Angevine, W. M. and K. Mitchell, 2001: Evaluation of the NCEP mesoscale Eta Model convective boundary layer for air quality applications. *Mon. Wea. Rev.*, **129**, 2761–2775.

Beljaars, A. C. M., 1994: The parametrization of surface fluxes in large-scale models under free convection. *Quart. J. Roy. Meteor. Soc.,* **121**, 255-270.

Bonan, G. B., S. Levis, L. Kergoat, and K. W. Oleson, 2002: Landscapes as patches of plant functional types: An integrating concept for climate and ecosystem models, *Global Biogeochem. Cycles*, **16(2)**, 1021, doi:10.1029/2000GB001360.

Borak, J., M. Jasinski, and R. Crago, 2005: Time series vegetation aerodynamic roughness fields estimated from modis observations. *Agricultural and Forest Meteorology.* **135,** 252-268.

Bou-Zeid, E., M. B. Parlange, and C. Meneveau, 2007: On the Parameterization of Surface Roughness at Regional Scales, *J. Atmos. Sci.,* **64**, 216-227.

Brock, F. V., K. C. Crawford, R. L. Elliott, G. W. Cuperus, S. J. Stadler, H. L. Johnson, and M. D. Eilts, 1995: The Oklahoma Mesonet: A technical overview, *J. Atmos. Oceanic Technol.*, **12**, 5 –19.

Brutsaert, W. 1982: *Evaporation into the Atmosphere: Theory, History, and Applications.* D. Reidel, 299 pp.

Brutsaert, Wilfried. 2005: *Hydrology - An Introduction*. Cambridge University Press, Cambridge, UK., 605 pp.

Chou M.-D., and M. J. Suarez, 1994: An efficient thermal infrared radiation parameterization for use in general circulation models. *NASA Tech. Memo 104606*, 3, 85 pp.

Courault, D., P. Drobinski, Y. Brunet, P. Lacarrere and C. Talbot, 2007: Impact of surface heterogeneity on a buoyancy-driven convective boundary layer in light winds, Boundary-Layer Meteor., 124, 383–403.

Crago, RD, 1998: Radiometric and equivalent isothermal surface temperatures, *Water Resour. Res.* **34(11),** 3017-3023.

Dickinson, R. E., and A. Henderson-Sellers, 1988: Modeling tropical deforestation: a study of GCM land-surface parameterizations. *Quart. J. Roy. Meteor. Soc.*. **114**, 439-462.

Dickinson R.E., A. Henderson-Sellers and P.J. Kennedy, 1993: Biosphere-Atmosphere Transfer Scheme (BATS) Version 1e as Coupled to the NCAR Community Climate Model. *National Center for Atmospheric Research (NCAR) Tech. Note, NCAR/TN-387+STR*, 72pp.

Dorman, J., and P. Sellers, 1989: A global climatology of albedo, roughness length and stomatal resistance for atmospheric general circulation models as represented by the Simple Biosphere model (SiB*). J. Appl. Meteor.*. **28**, 833-855.

Driese, K. and W. A. Reiners, 1997: Aerodynamic roughness parameters for semi-arid natural shrub communities of Wyoming, USA , *Agricul. and For. Meteor.,* **88**(1-4),1-14.

Eagleson, P.S., 2000: *Ecohydrology.* Cambridge University Press, 443 pp.

Friedl, M. A., McIver, D. K., Hodges, J. C. F., Zhang, X. Y., Muchoney, D., Strahler, A. H., Woodcock C., Gopal S., Schneider A., Cooper A., Baccini A., Gao F., and C. Schaaf, 2002: Global land cover mapping from MODIS: Algorithms and early results. *Remote Sens. Environ.*, **83**, 287−302.

Hahmann, A., and R. Dickinson, 1997: RCCM2-BATS model over tropical South America: application to tropical deforestation. *J Climate*, **10**, 1944–1964.

Hahmann, A., and R. Dickinson, 2001: A Fine-Mesh Land Approach for General Circulation Models and Its Impact on Regional Climate, *J Climate*, **14**, 1634-1646.

Horst, T., 2002: IHOP02: Chronological Logbook Entries 325 & 326. Available online at [http://www.eol.ucar.edu/isf/projects/ihop_2002/isff/logbook/Logbook_Contents.html.]

Huang., H., B. Stevens, and S. Margulis, 2008: Application of Dynamic Subgrid-scale Models for Large-eddy Simulation of the Daytime Convective Boundary Layer over Heterogeneous Surfaces, Journal., *Bound.-Layer Meteor.,* **126(3)**, 327-348.

Janjić, Z. I., 1994: The step-mountain eta coordinate model: Further developments of the convection, viscous sublayer, and turbulence closure schemes. *Mon. Wea. Rev*, **122**, 927–945.

Janjić, Z. I., 2002: Nonsingular Implementation of the Mellor-Yamada Level 2.5 Scheme in the NCEP Meso model. *NCEP Office Note*. No. 437, 61 pp.

Jasinski, M.F., J. Borak, and R.D. Crago, 2005: Bulk Surface Momentum Parameters for Satellite-Derived Vegetation fields. *Agric. and Forest Meteor.* **133**, 55-68.

Jasinski, M.F., Crago, R.D., 1999. Estimation of vegetation aerodynamic roughness of natural regions using frontal area density determined from satellite imagery. *Agric. and Forest Meteor.,* **94**, 65-77.

Kang, S.-L., K. J. Davis, and M. LeMone, 2007: The Effects of Surface Heterogeneity on the Fair-Weather convective Atmospheric boundary layer. *J. Atmos. Sci.,* **65,** 3197-3213.

Kang, S.-L., K. J. Davis, 2008: Observations of the ABL structures over a heterogeneous surface during IHOP_2002. *J. Hydrometeor.,* **8,** 221–244.

Klink, K., 1992: Evaluating climate-vegetation interactions at climate model sub-grid scales. *Publ. Climatal*. **45**(1), 57pp.

Kumar, S. V., C. D. Peters-Lidard, Y. Tian, P. R. Houser, J. Geiger, S. Olden, L. Lighty, J. L. Eastman, B. Doty, P. Dirmeyer, J. Adams, K. Mitchell, E. F. Wood and J. Sheffield, 2004: Land information system: An Interoperable Framework for High Resolution Land Surface Modeling. *Environmental Modelling & Software*, **21**, 1402-1415.

Lean J., and P. Rowntree, 1997: Understanding the sensitivity of a GCM simulation of Amazonian deforestation to the specification of vegetation and soil characteristics. *J Climate* **10**, 1216–1235.

Lin, C-L., and J. Glendening, 2002: Large Eddy Simulation of Internal Boundary Layers Created by a Change in Surface Roughness. *J. Atmos. Sci.,* **59**, 2479-2497.

Lin, Y.-L., R. D. Farley, and H. D. Orville, 1983: Bulk parameterization of the snow field in a cloud model. *J. Climate Appl. Meteor*., **22**, 1065-1092.

Lindroth, A., 1993: Aerodynamic and canopy resistance of shortrotation forest in relationship to leaf area index and climate. *Bound.-Layer Meteor.,* **66,** 265–279.

Loveland T. R. and A.S. Belward, 1997: The IGBP-DIS global 1km land cover data set, DISCover: first results. *Int. J. of Remote Sensing,* **18**(7), 3289-3295.

Lu, L., Liu, S., Z. Xu, K. Yang, X. Cai, L. Jiaand, and J. Wang, 2009: The characteristics and parameterization of aerodynamic roughness length over heterogeneous surfaces. *Adv Atmos Sciences*. **26(1)**, 180-190.

Massman, W.J., 1997: An analytical one-dimensional model of momentum transfer by vegetation of arbitrary structure. *Bound.-Layer Meteor.* **83**, 407–421.

Milly, P. , and A. Shmakin, 2002**:** Global modeling of land water and energy balances. Part II: Land-characteristic contributions to spatial variability**.** *J. Hydrometeorology*, **3(3)**, 301-310.

Mitchell, K. E., and Coauthors, 2004: The multi-institution North American Land Data Assimilation System (NLDAS): Utilizing multiple GCIP products and partners in a

continental distributedhydrological modeling system. *J. Geophys. Res.,* **109**, D07S90, doi:10.1029/2003JD003823.

Mlawer, E. J., S. J. Taubman, P. D. Brown, M. J. Iacono, and S. A. Clough, 1997: Radiative trans-fer for inhomogeneous atmosphere: RRTM, a validated correlated-k model for the long-wave. *J. Geophys. Res.,* **102(D14)**, 16663-16682.

Nakai, T., and Coauthors, 2008: Parameterisation of aerodynamic roughness over boreal, cool- and warm-temperate forests, *Agric and For Mete*or, **148(12),** 1916-1925.

Raupach, M.R., 1992: Drag and drag partition on rough surfaces. *Boundary Layer Meteorology,* **60**, 375-395.

Raupach, M.R., 1994: Simplified expressions for vegetation roughness length and zero-plane displacment as functions of canopy height and area index. *Bound.-Layer Meteor.* **71**, 211-216.

Raupach, M.R., 1995: Simplified expressions for vegetation roughness length and zero-plane displacment as functions of canopy height and area index. *Bound.-Layer Meteor.* **71**, 211-216, Corrigenda.

Rutledge, S. A., and P. V. Hobbs, 1984: The mesoscale and microscale structure and organization of clouds and precipitation in midlatitude cyclones. XII: A diagnostic modeling study of precipitation development in narrow cloud-frontal rainbands. *J. Atmos. Sci.,* **20**, 2949-2972.

Saachi, S., and E. Rodriguez, 1999: Relating Vegetation Aerodynamic Roughness Length to. Interferometric SAR Measurements. *Proc. IEEE 1999 International Geoscience And Remote Sensing Symposium. Hamburg, Germany, p. 1643-1645.*

Schaudt, K.J., Dickenson, R.E., 2000: An approach to deriving roughness length and zero-plane displacement height from satellite data, prototyped with BOREAS data. *Agric. and Forest Meter.,* **104**, 143-155.

Sellers, P.J., 1992: Land surface process modeling. In *Climate System Modeling*, Trenberth K (ed.). Cambridge University Press: 451–490.

Sellers, P. J., Berry, J. A., Collatz, G. J., Field, C. B., and F.G. Hall, 1992: Canopy Reflectance, Photosynthesis and Transpiration. III. A Re Analysis Using Improved Leaf Models and a New Canopy Integration Scheme, *Remote Sens. Environ*. **42**, 187–216.

Skamarock, W. C., J. B. Klemp, J. Dudhia, D. O. Gill, D. M. Barker, W. Wang, and J. G. Powers, 2005: A description of the Advanced Research WRF Version 2. *NCAR Tech Notes-468+STR.*

Sud Y., J. Shukla, Y. Mintz, 1988: Influence of land surface roughness on atmospheric circulation and precipitation: a sensitivity study with a general circulation model. *J Appl Meteor.* **27**, 1036–1054.

Sud, Y. and W. Smith, 1985: The Influence of Surface Roughness of Deserts on the July Circulation.A Numerical Study, *Bound.-Layer Meteor.*. **33**, 15-49.

Sud, Y. C., W.K-M Lau, G. K.Walker, G. E. Liston, and P.J. Sellers, 1996: Biogeophysical Consequences of a Tropical Deforestation Scenario: A GCM Simulation Study. *J. Climate,* **9**, 3225–3247.

United States Department of Agriculture. Natural Resources Conservation Service, 1994: State Soil Geographic (STATSGO) Data Base, Data use information. Pub. 1492, 113 pp.

Weaver, C.P., and R. Avissar, 2001: Atmospheric disturbances caused by human modification of the landscape. *Bull. Amer. Meteorol. Soc.,* **82**, 269-281.

Weaver, C.P. , 2004: Coupling between Large-Scale Atmospheric processes and Mesoscale land-Atmosphere Interactions in the U.S. Southern Great Plains during Summer. Part II: Mean Impacts of the Mesoscale. *J. Hydrometeor.,* **5,** 1247-1258.

Weisman M. L., C. Davis, W. Wang, K. W. Manning, and J. B. Klemp, 2008: Experiences with 0–36-h Explicit Convective Forecasts with the WRF-ARW Model. *Weather and Forecasting*, **23**, 407-437.

Yang, R., M.A. Friedl, 2003: Determination of roughness lengths for heat and momentum over boreal forests. Boundary-Layer Meteorol. **107**, 581–603.

Zeng, X., M. Shaikh, Y. Dai, R. Dickinsin, and R Myneni, 2002: Coupling of the Common Land Model to the NCAR Community Climate Model. *J. Climate* **15**, 1832-1854.

Zeng , X. and A.Wang, 2008: A Consistent Parameterization of Roughness Length and Displacement Height for Sparse and Dense Canopies in Land Models. *J. Hydrometeor.,* **8(4)** 730-737.

Zhang, D. and R. A. Anthes, 1982: A high-resolution model of the planetary boundary layer Sensitivity tests and comparisons with SESAME-79 data. *J. Appl. Meteor.*, **21**(11), 1594-1609.

Zhang, H., A. Henderson-Sellers, and K. McGuffie, 1996: Impacts of tropical deforestation. Part I: Process analysis of local climatic change. *J. Climate,* **9,** 1497–1517.

Zhao, M. and A.J. Pitman, 2002: The regional scale impact of land cover change simulated with a climate model, *Int. J. Climatology*, **22**, 271-290.

Zhong, L., H. Li, and K. Zhang, 2007: New expressions for the surface roughness length and displacement height in the atmospheric boundary layer. *Chinese Physics*, **16(07)**, 2033-2039.

Zhong, S., and J.C. Doran, 1998: An evaluation of the importance of surface flux variability on GCM-scale boundary layer characteristics using realistic meteorological and surface forcing. *J. Climate*, **11**, 2774–2788.

Zilitinkevich, S., I. Mammarella, A. Baklanov, and S. Joffre, 2008: The Effect of Stratification on the Aerodynamic Roughness Length and Displacement Height. *Boundary-Layer Meteorol*, **129**, 179–190.

List of Figures

wetland, 12 – Cropland, 13 – Urban, 14 – Cropland and natural vegetation mosaic, 15 – Snow and ice, 16 – Barren or sparsely vegetated.

FIG. 5. Diurnal evolution of the temperature BIAS averaged over all stations. HETER BIAS is represented by the solid line, CLIMO by the short dashed line, and CONTR by the long dashes. HETER generally exhibits the least cool BIAS during the daytime hours but seems to have a slightly higher warm BIAS at night.

FIG. 6. POD evaluated at every hour of the integration. HETER is represented by the solid line, CLIMO by the short dashed line, and CONTR by the long dashes. Results indicate that HETER exhibits about the same POD as CLIMO and CONTR, although it is slightly higher initially and over time.

FIG. 7a-b. Domain averaged wind speed at 2m (7a) and differences in domain averaged wind speed (7b) for the FULL domain over the 96 hour integration period. Results indicate that roughness heterogeneity increased modeled daytime wind speed by about 5 %, while it decreasing nighttime wind speed by the same amount.

FIG. 8a-b. Domain averaged wind speed at 2m (8a) and differences in domain averaged wind speed (8b) for the GRASS domain over the 96 hour integration period. Results indicate that differences with HETER are generally greatest. Roughness heterogeneity exhibits less effect during the middle of the simulations characterized by intense convection.

FIG. 9. Domain averaged wind speed at 2m (9a) and differences in domain averaged wind speed (9b) for the MIXED domain over the 96 hour integration period. Results indicate that roughness heterogeneity increased modeled daytime wind speed by about 10%, with significantly less impact during nighttime.

FIG. 10. Domain averaged PBL height (10a) and differences in domain averaged PBL height (10b) for the FULL domain over the 96 hour integration period. Results indicate that roughness heterogeneity increased modeled daytime PBL height by about 5 %, while it decreasing nighttime heights.

FIG. 11. Domain averaged PBL height (11a) and differences in domain averaged PBL height (11b) for the GRASS domain over the 96 hour integration period. Results indicate that roughness heterogeneity impacts this domain by only several percent.

FIG. 12. Domain averaged PBL height (12a) and differences in domain averaged PBL height (12b) for the MIXED domain over the 96 hour integration period. Results indicate that roughness heterogeneity increased modeled daytime PBL height by up to 10% during daytime periods.

FIG. 13: PDF of vertical motion for the FULL domain, computed for 20GMT for the 4 days at 726m AGL. Results indicate that HETER demonstrates a broadening of the distribution, as well as a 25% decrease in peak values, when compared to the low heterogeneity CLIMO and CONTR cases.

FIG. 14. PDF of vertical motion for the GRASS domain, computed for 20GMT for the 4 days at 726m AGL. Results indicate that HETER demonstrates only slight broadening of the distribution, as well as less than 15% decrease in peak values, when compared to the low heterogeneity CLIMO and CONTR cases.

FIG. 15. PDF of vertical motion for the MIXED domain, computed for 20GMT for the 4 days at 726m AGL. Results indicate that HETER demonstrates a broadening of the distribution, as well as 30-35% decrease in peak values, when compared to the low heterogeneity CLIMO and CONTR cases.

FIG. 16. FULL domain 4-day averaged TKE profile at 18GMT. An impact of 10 to 20% is shown throughout vertical profile up to 1655m, although the greatest absolute differences (~0.3 m^2/s^2) occur at the second level (46m).

FIG. 17. GRASS domain 4-day averaged TKE profile at 18GMT. The greatest difference of ~3% occurs at the second level (46m), although the overall impact is significantly less compared to the FULL domain.

FIG. 18. MIXED domain 4-day averaged TKE profile at 18GMT. The greatest difference of ~8% occurs at the second level (46m), although the overall impact is less compared to the FULL domain.

FIG. 19. FULL domain averaged TKE (19a) and differences in TKE (19b) at 40m AGL over the 4 day integration. Results indicate that TKE is enhanced by about 10% during mid-day, but reversed in the evening.

FIG. 20. GRASS domain averaged TKE (20a) and differences in TKE (20b) at 40m AGL over the 4 day integration. Results indicate that TKE is enhanced during mid-day but suppressed in the evening, but to a much lesser degree than in FULL and MIXED.

FIG. 21. MIXED domain averaged TKE (21a) and differences in TKE (21b) at 40m AGL over the 4 day integration. Results indicate that TKE is enhanced during mid-day by 10-20%.

Figures

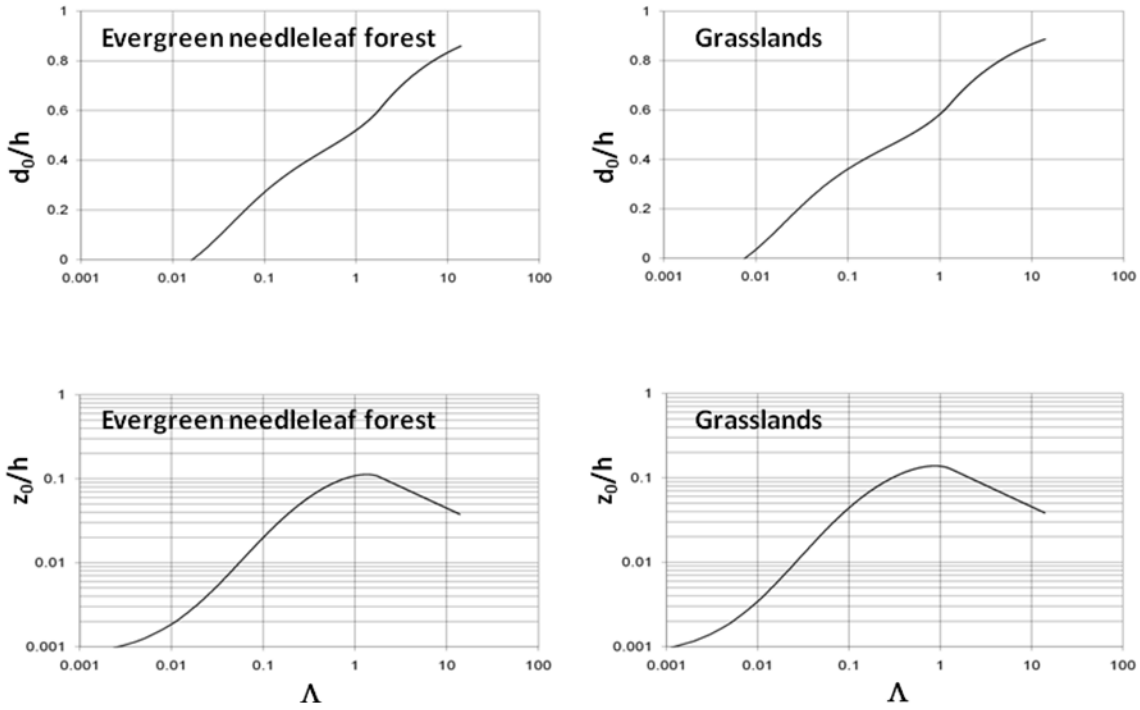

FIG. 1. Typical theoretical plot of d_0/h and z_0/h verses canopy area index, Λ, for the land cover types evergreen needleleaf forest (left side of page) and grasslands (right side of page). Similar plots have been developed for all the principal IGBP land classes (after Jasinski et al, 2005).

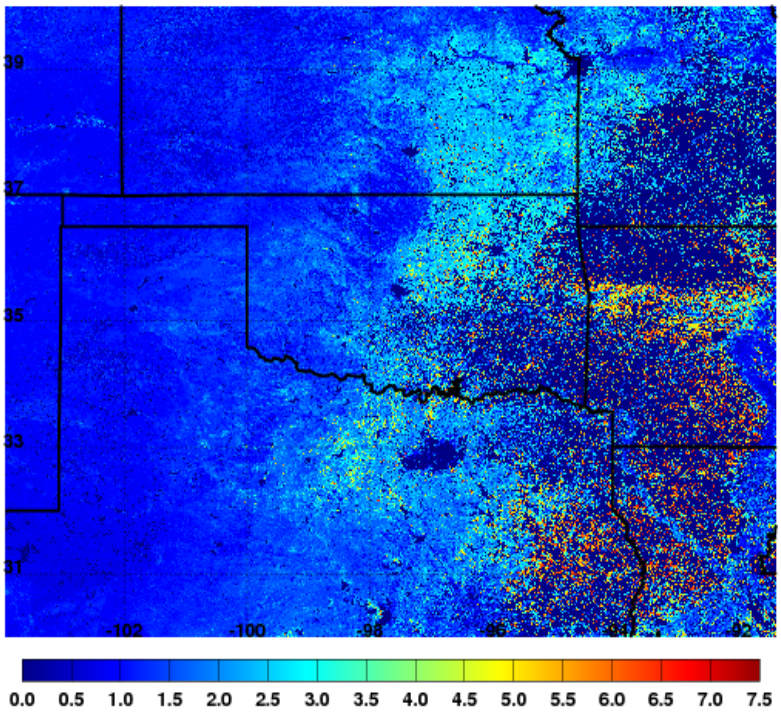

FIG. 2. Canopy Area Index, Λ, for MODIS compositing period June 2-9, 2002, in meters. Λ was computed on a pixel-by-pixel basis using MODIS data products as described in Section 2.b and Equations 6 and 7. Λ represents the total surface area of all momentum absorbing elements in the canopy.

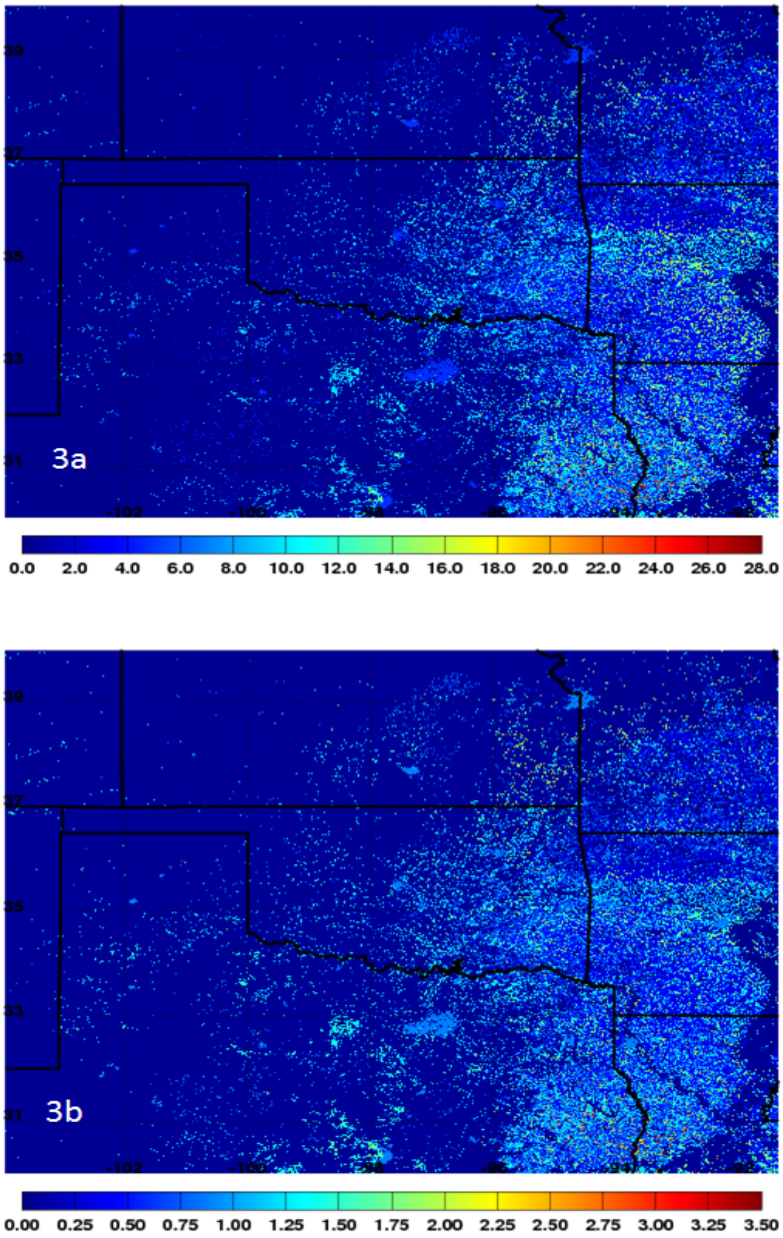

FIGS. 3a and b. Estimated d_0 and z_0 in meters, respectively, for MODIS compositing period June 2-9, 2002, in meters. Roughness maps were developed by applying MODIS-derived Canopy Area Index on a pixel by pixel basis to a modified version of Raupach's formulation.

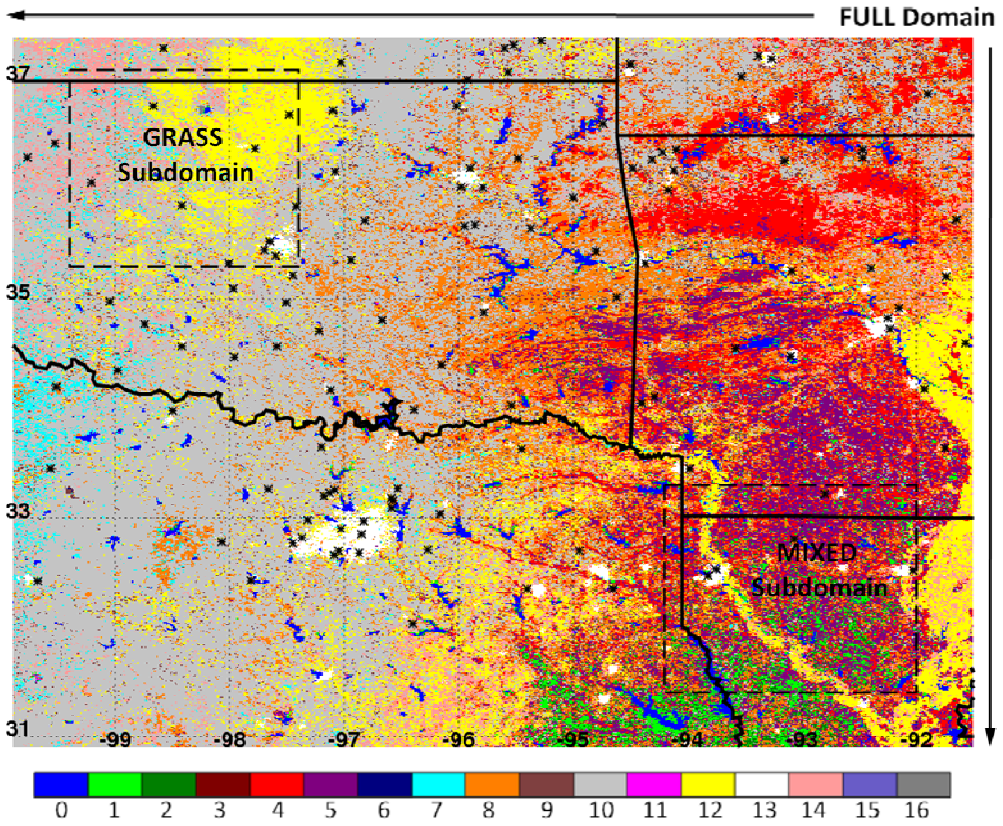

FIG. 4. Location map and IGBP land cover type for the FULL domain and the GRASS and MIXED subdomains. Meteorological stations indicated by ∗. Land cover type key: 0- Water, 1 – Evergreen needleleaf forest, 2 – Evergreen broadleaf forest, 3 – Deciduous needleleaf forest, 4-Deciduous broadleaf forest, 5 – Mixed forest, 6 – Closed shrubland, 7 - Open shrubland, 8 – Woody savanna, 9 – Savanna, 10 – Grassland, 11 – Permanent wetland, 12 – Cropland, 13 – Urban, 14 – Cropland and natural vegetation mosaic, 15 – Snow and ice, 16 – Barren or sparsely vegetated.

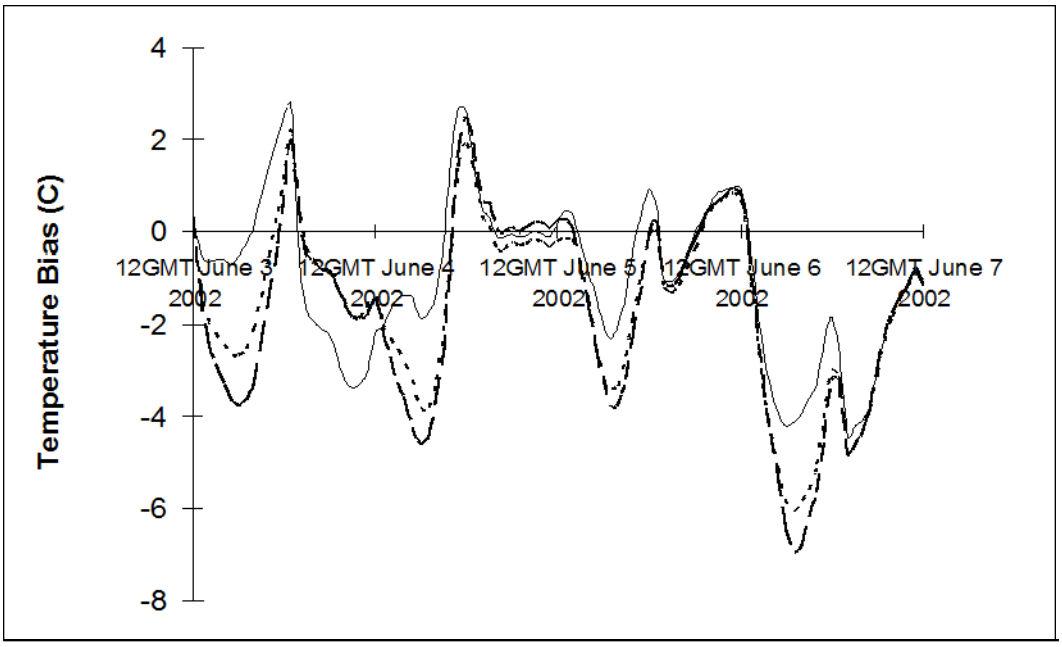

FIG. 5. Diurnal evolution of the temperature BIAS averaged over all stations. HETER BIAS is represented by the solid line, CLIMO by the short dashed line, and CONTR by the long dashes. HETER generally exhibits the least cool BIAS during the daytime hours but seems to have a slightly higher warm BIAS at night.

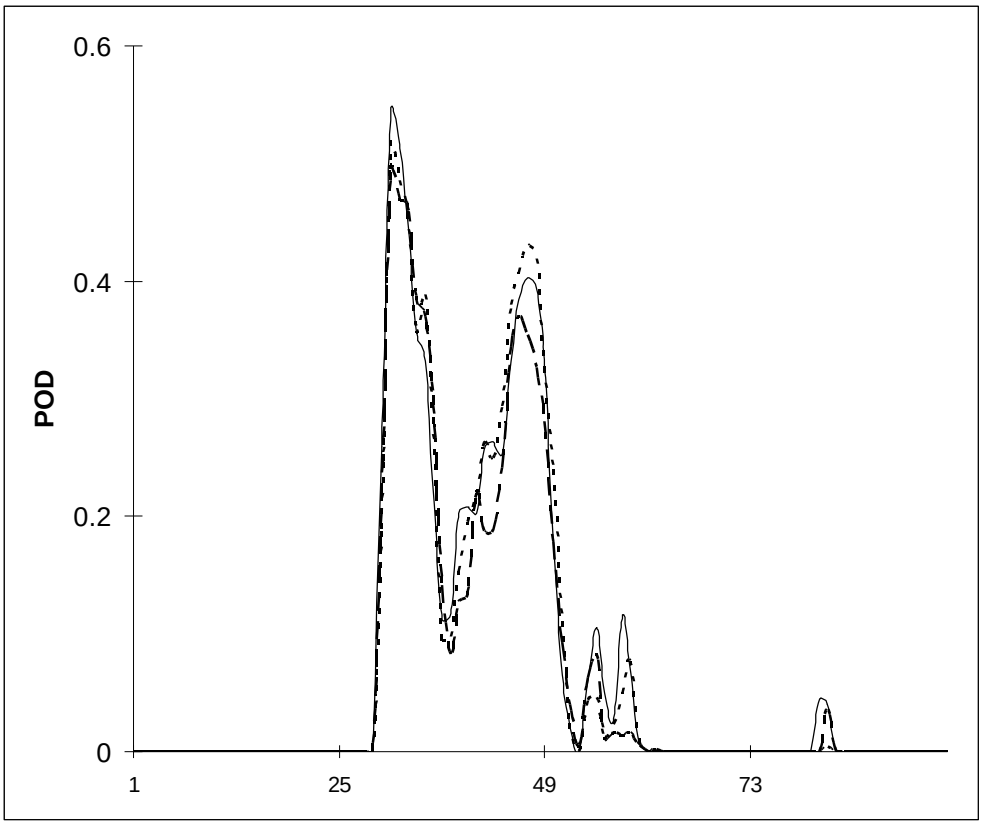

FIG. 6. POD evaluated at every hour of the integration. HETER is represented by the solid line, CLIMO by the short dashed line, and CONTR by the long dashes. Results indicate that HETER exhibits about the same POD as CLIMO and CONTR, although it is slightly higher initially and over time.

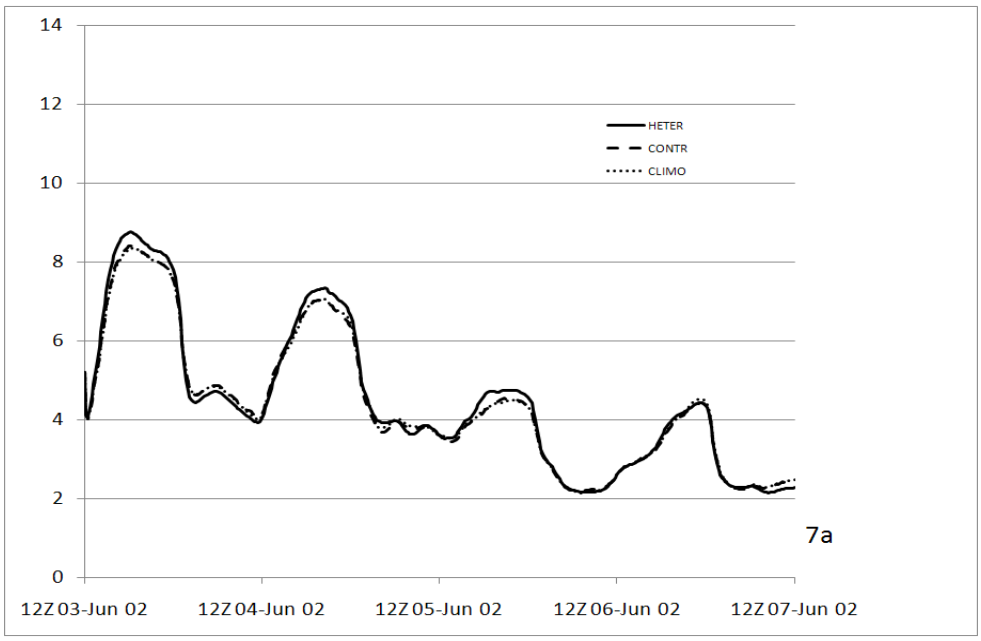

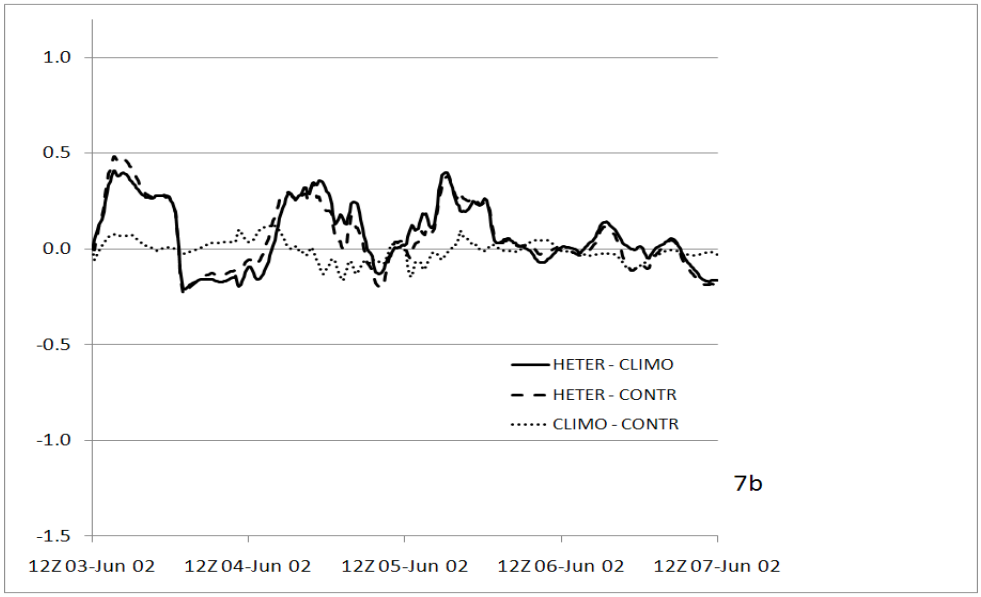

FIG. 7a-b. Domain averaged wind speed at 2m (7a) and differences in domain averaged wind speed (7b) for the FULL domain over the 96 hour integration period. Results indicate that roughness heterogeneity increased modeled daytime wind speed by about 5 %, while it decreasing nighttime wind speed by the same amount.

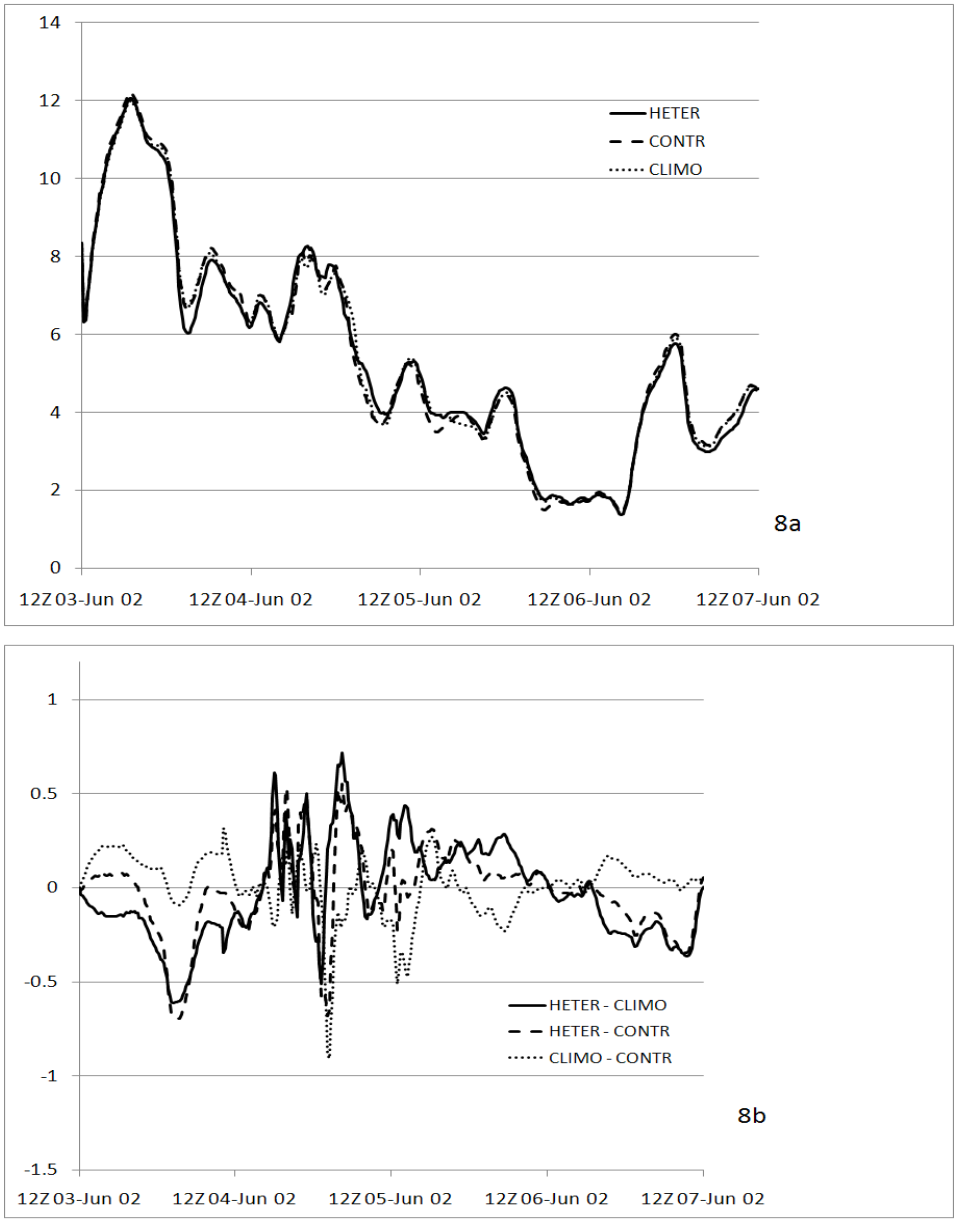

FIG. 8a-b. Domain averaged wind speed at 2m (8a) and differences in domain averaged wind speed (8b) for the GRASS domain over the 96 hour integration period. Results indicate that differences with HETER are generally greatest. Roughness heterogeneity exhibits less effect during the middle of the simulations characterized by intense convection.

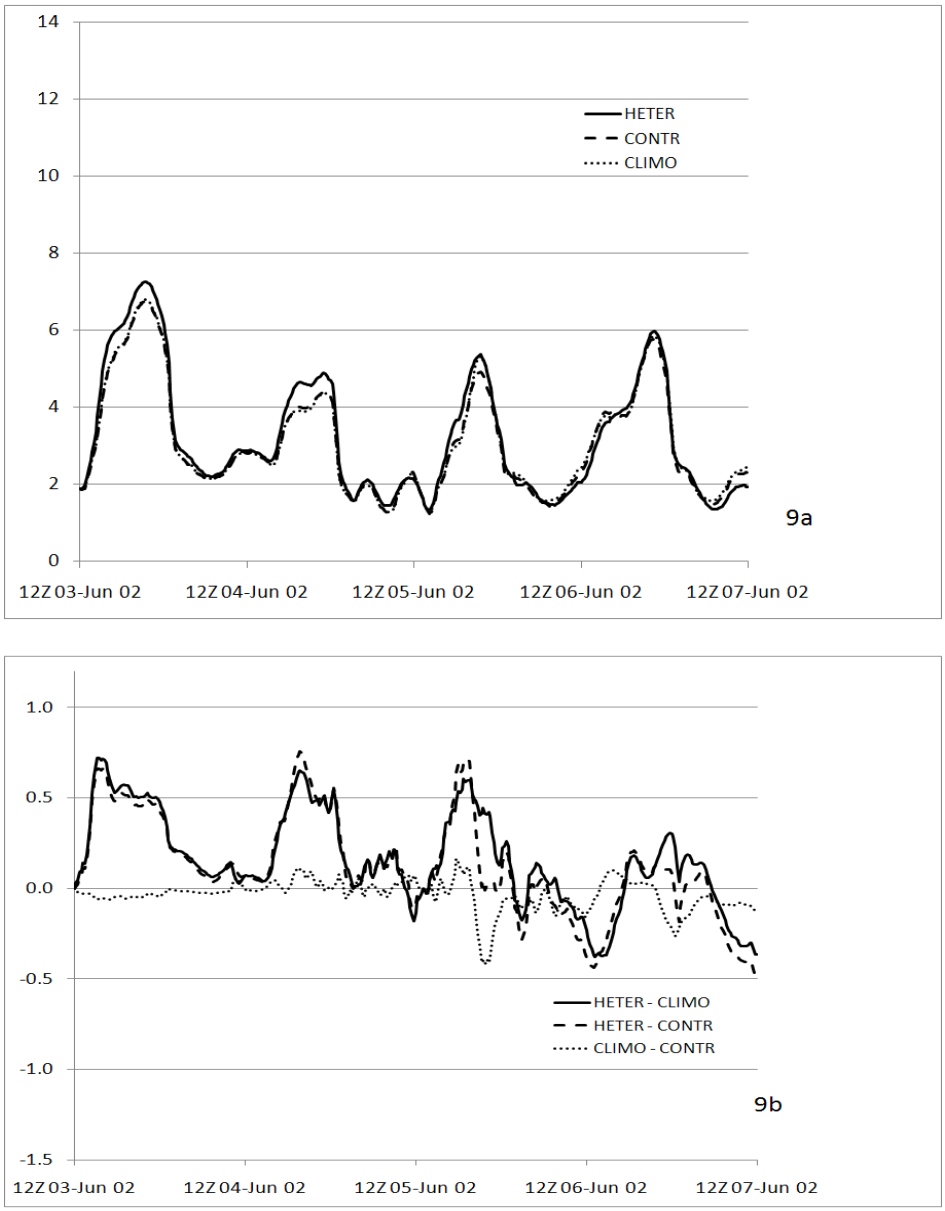

FIG. 9. Domain averaged wind speed at 2m (9a) and differences in domain averaged wind speed (9b) for the MIXED domain over the 96 hour integration period. Results indicate that roughness heterogeneity increased modeled daytime wind speed by about 10%, with significantly less impact during nighttime.

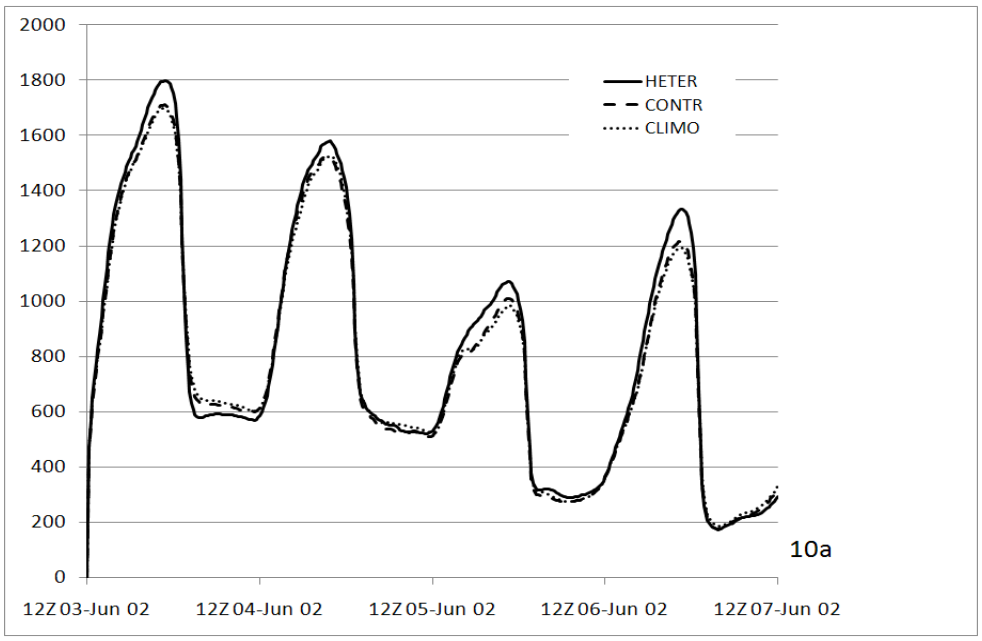

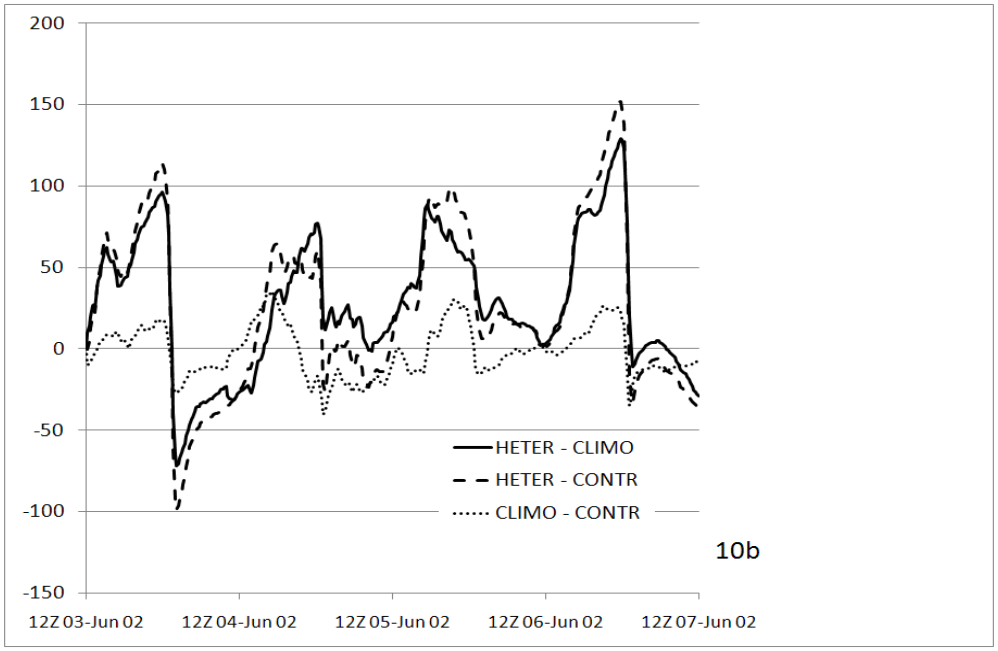

FIG. 10. Domain averaged PBL height (10a) and differences in domain averaged PBL height (10b) for the FULL domain over the 96 hour integration period. Results indicate that roughness heterogeneity increased modeled daytime PBL height by about 5 %, while it decreasing nighttime heights.

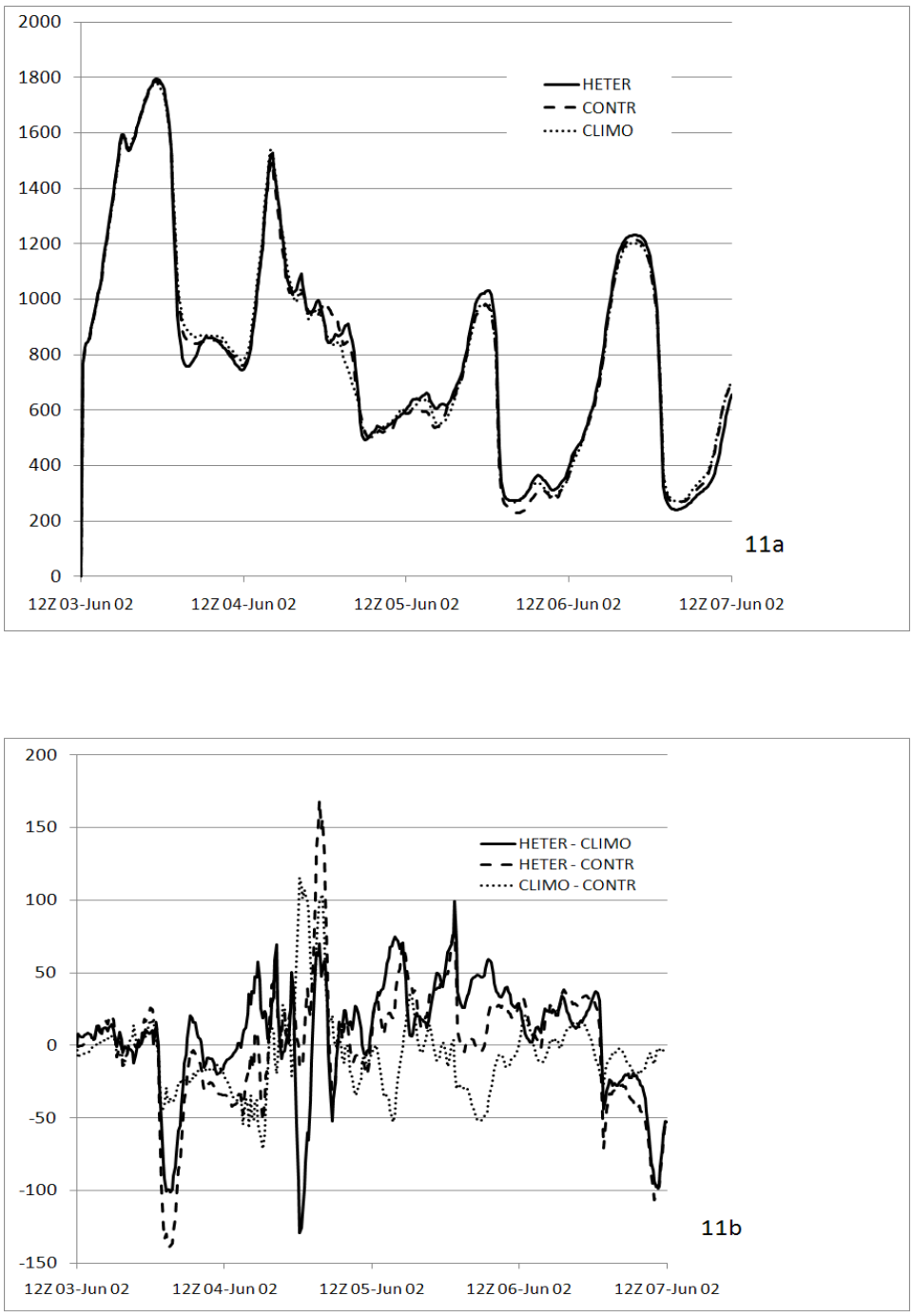

FIG. 11. Domain averaged PBL height (11a) and differences in domain averaged PBL height (11b) for the GRASS domain over the 96 hour integration period. Results indicate that roughness heterogeneity impacts this domain by only several percent.

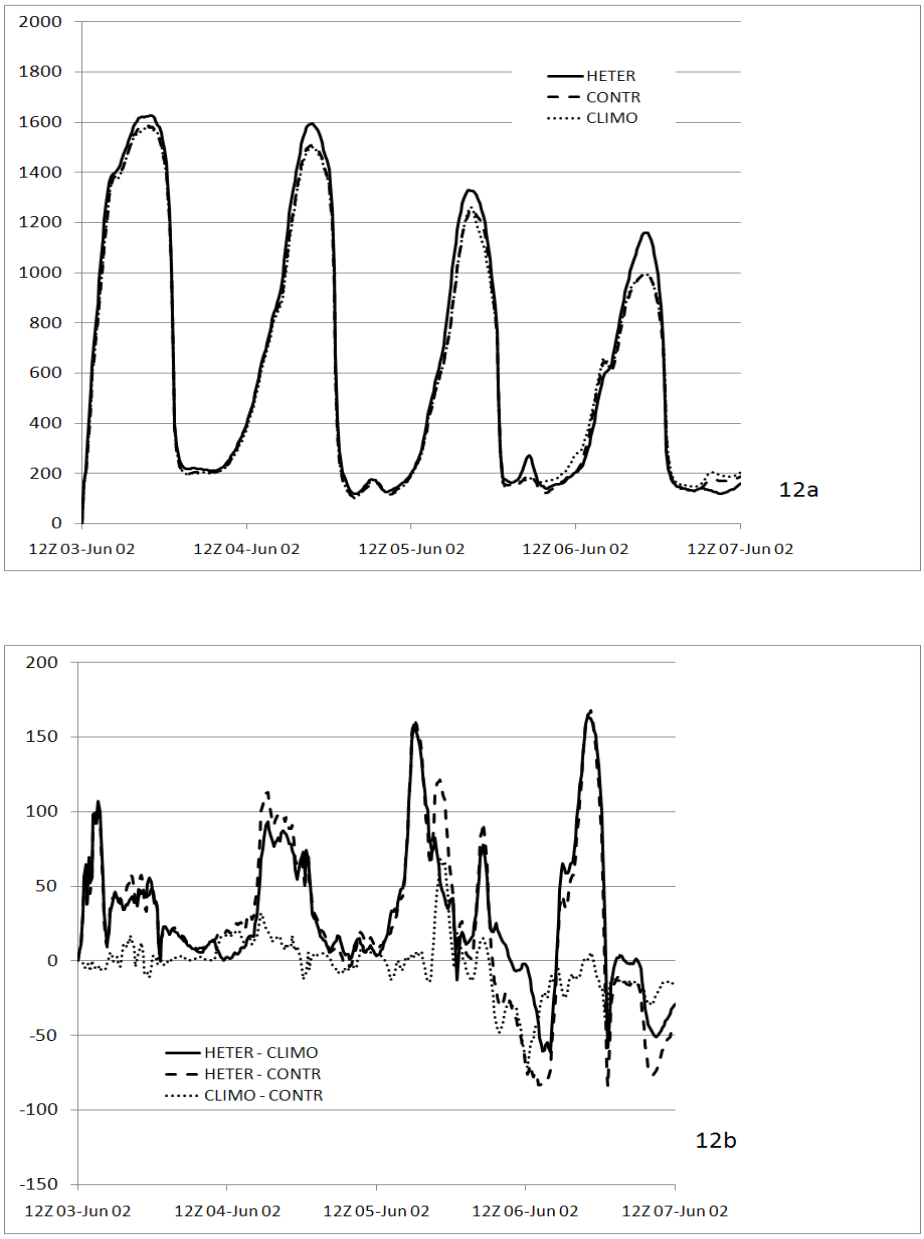

FIG. 12. Domain averaged PBL height (12a) and differences in domain averaged PBL height (12b) for the MIXED domain over the 96 hour integration period. Results indicate that roughness heterogeneity increased modeled daytime PBL height by up to 10% during daytime periods.

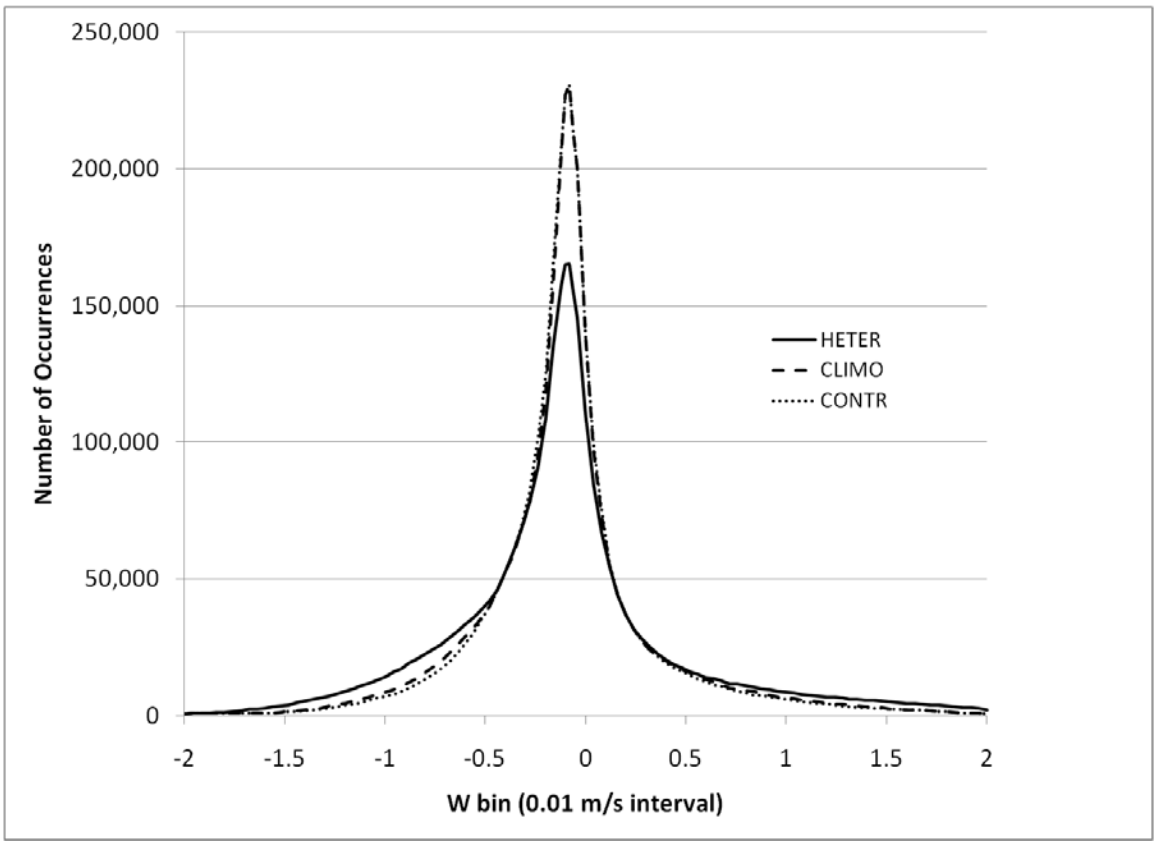

FIG. 13: PDF of vertical motion for the FULL domain, computed for 20GMT for the 4 days at 726m AGL. Results indicate that HETER demonstrates a broadening of the distribution, as well as a 25% decrease in peak values, when compared to the low heterogeneity CLIMO and CONTR cases.

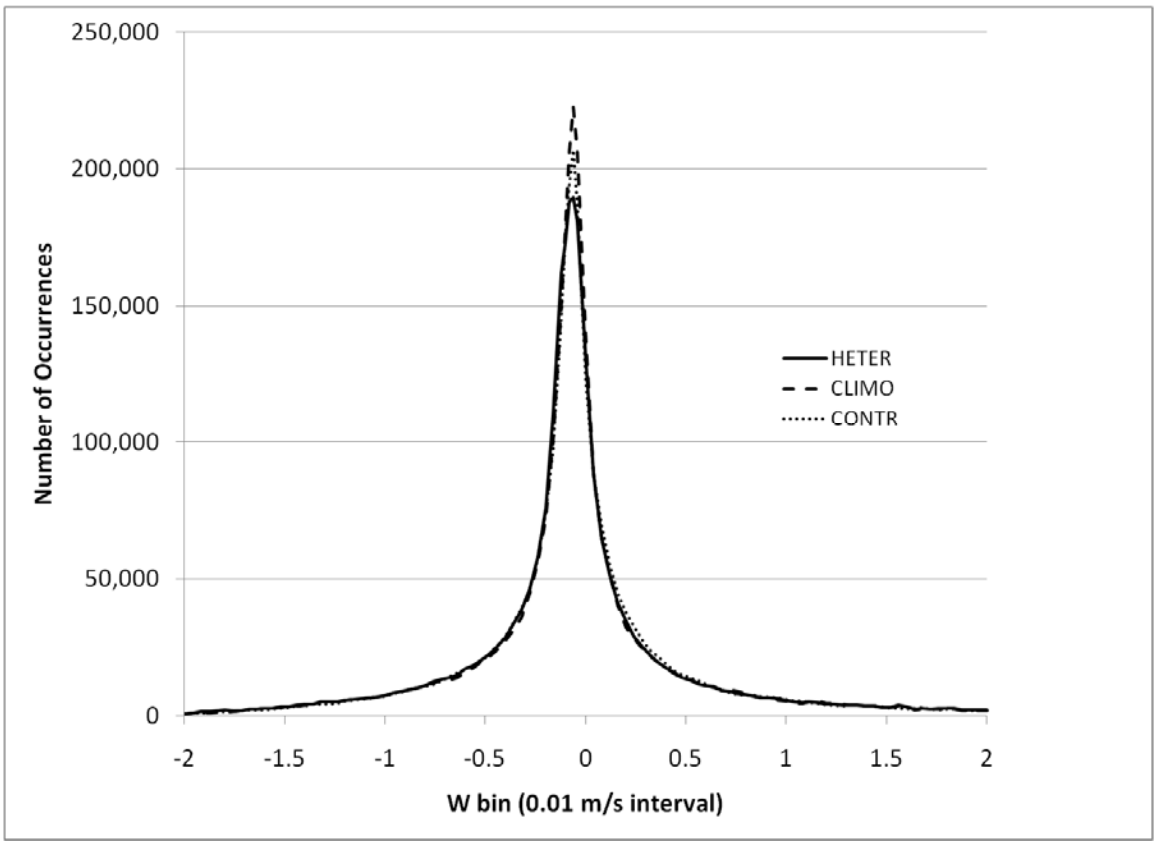

FIG. 14. PDF of vertical motion for the GRASS domain, computed for 20GMT for the 4 days at 726m AGL. Results indicate that HETER demonstrates only slight broadening of the distribution, as well as less than 15% decrease in peak values, when compared to the low heterogeneity CLIMO and CONTR cases.

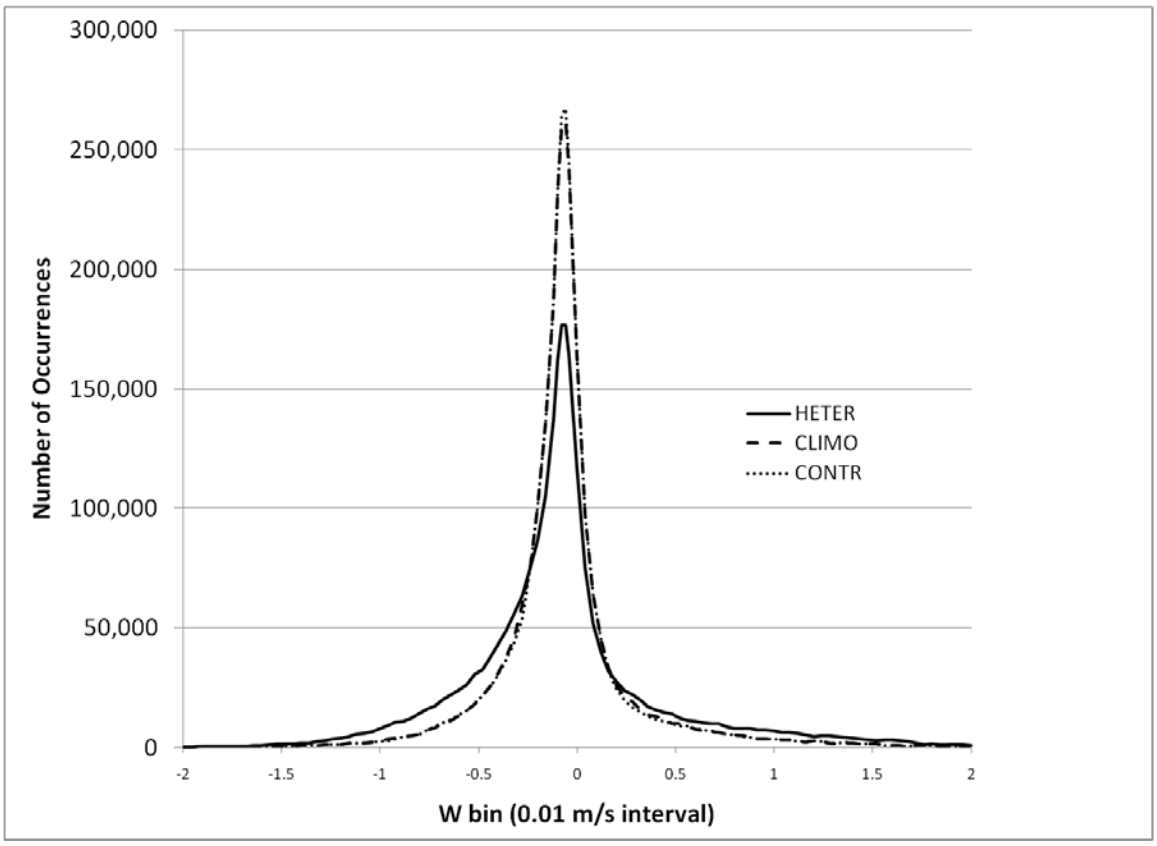

FIG. 15. PDF of vertical motion for the MIXED domain, computed for 20GMT for the 4 days at 726m AGL. Results indicate that HETER demonstrates a broadening of the distribution, as well as 30-35% decrease in peak values, when compared to the low heterogeneity CLIMO and CONTR cases.

.

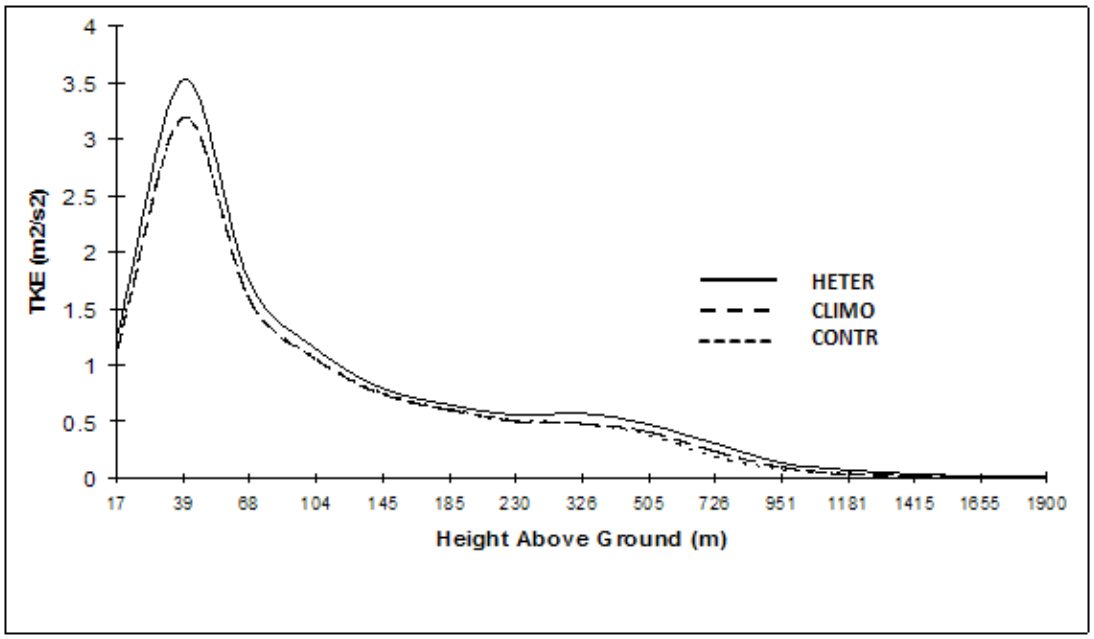

FIG. 16. FULL domain 4-day averaged TKE profile at 18GMT. An impact of 10 to 20% is shown throughout vertical profile up to 1655m, although the greatest absolute differences (~0.3 m^2/s^2) occur at the second level (46m).

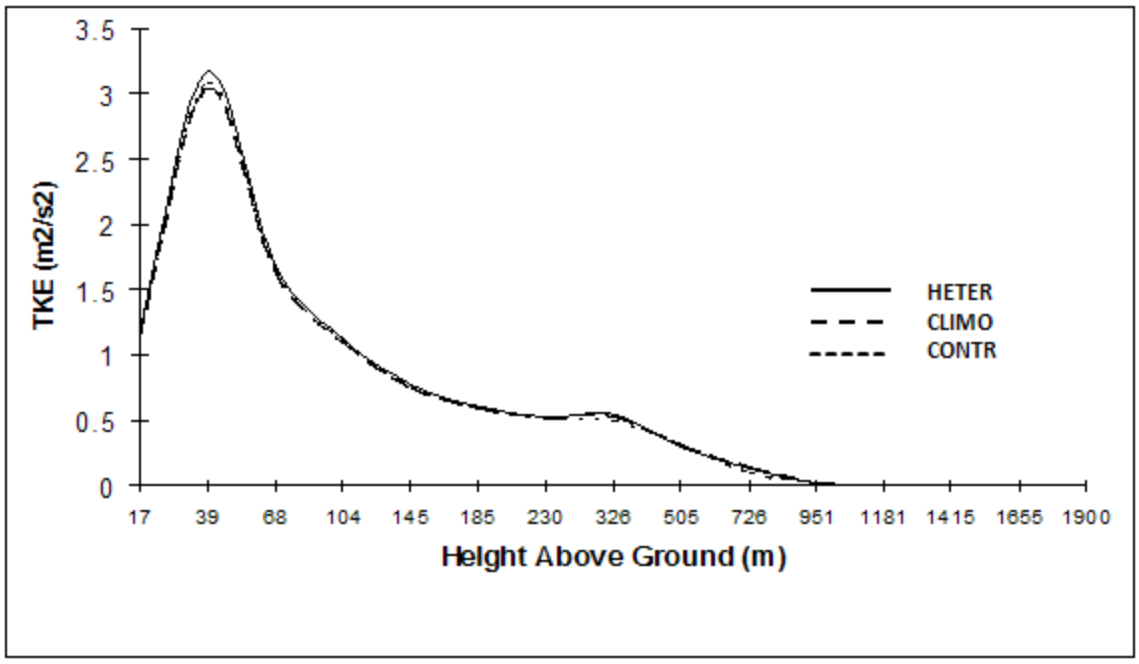

FIG. 17. GRASS domain 4-day averaged TKE profile at 18GMT. The greatest difference of ~3% occurs at the second level (46m), although the overall impact is significantly less compared to the FULL domain.

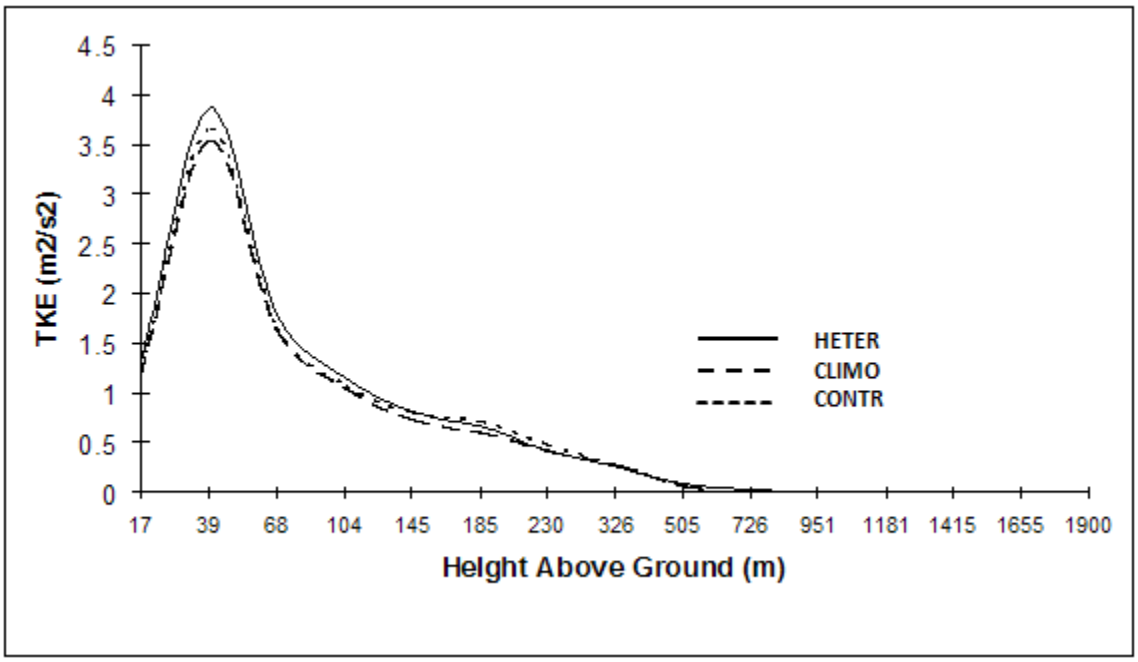

FIG. 18. MIXED domain 4-day averaged TKE profile at 18GMT. The greatest difference of ~8% occurs at the second level (46m), although the overall impact is less compared to the FULL domain.

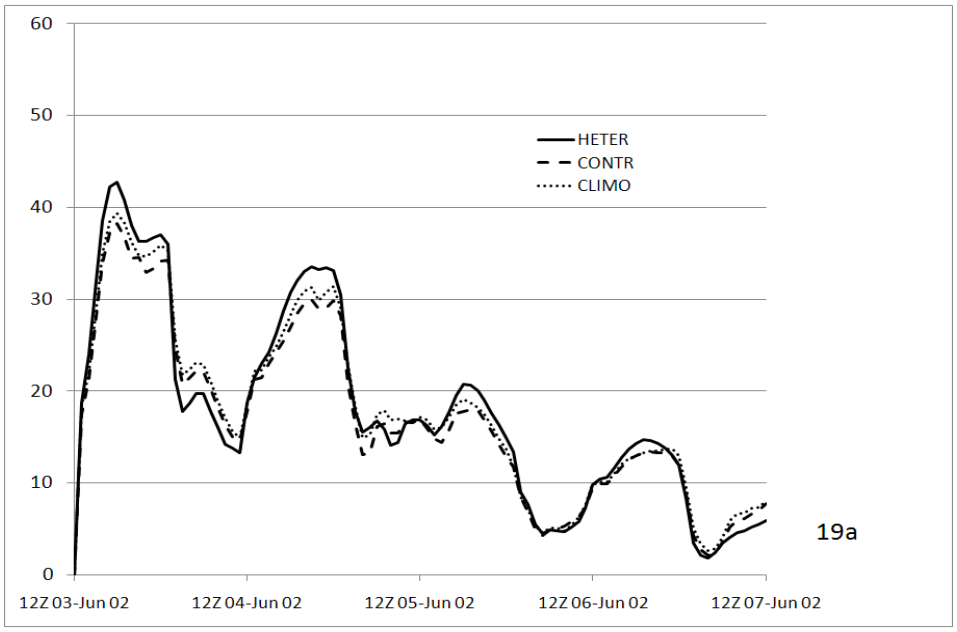

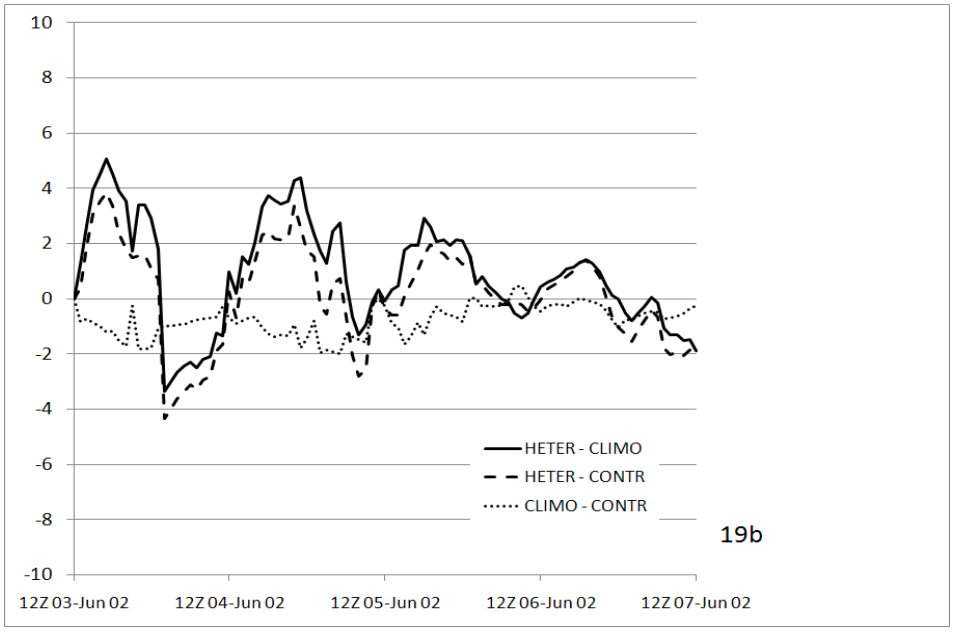

FIG. 19. FULL domain averaged TKE (19a) and differences in TKE (19b) at 40m AGL over the 4 day integration. Results indicate that TKE is enhanced by about 10% during mid-day, but reversed in the evening.

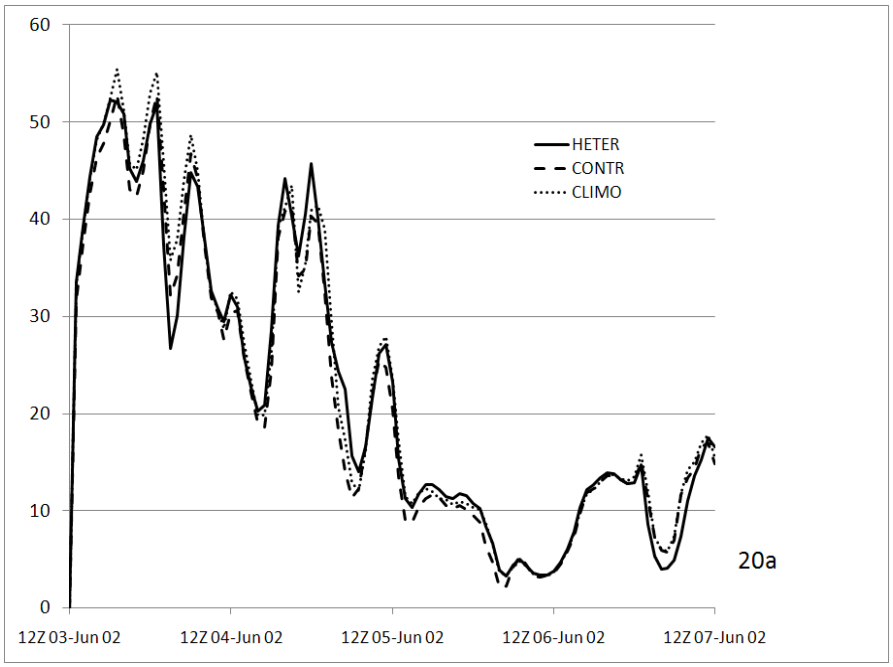

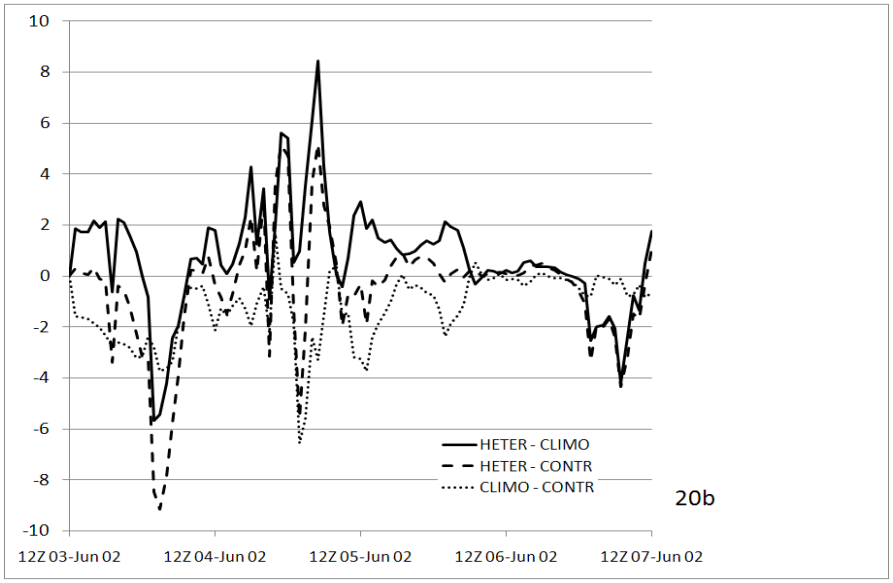

FIG. 20. GRASS domain averaged TKE (20a) and differences in TKE (20b) at 40m AGL over the 4 day integration. Results indicate that TKE is enhanced during mid-day but suppressed in the evening, but to a much lesser degree than in FULL and MIXED.

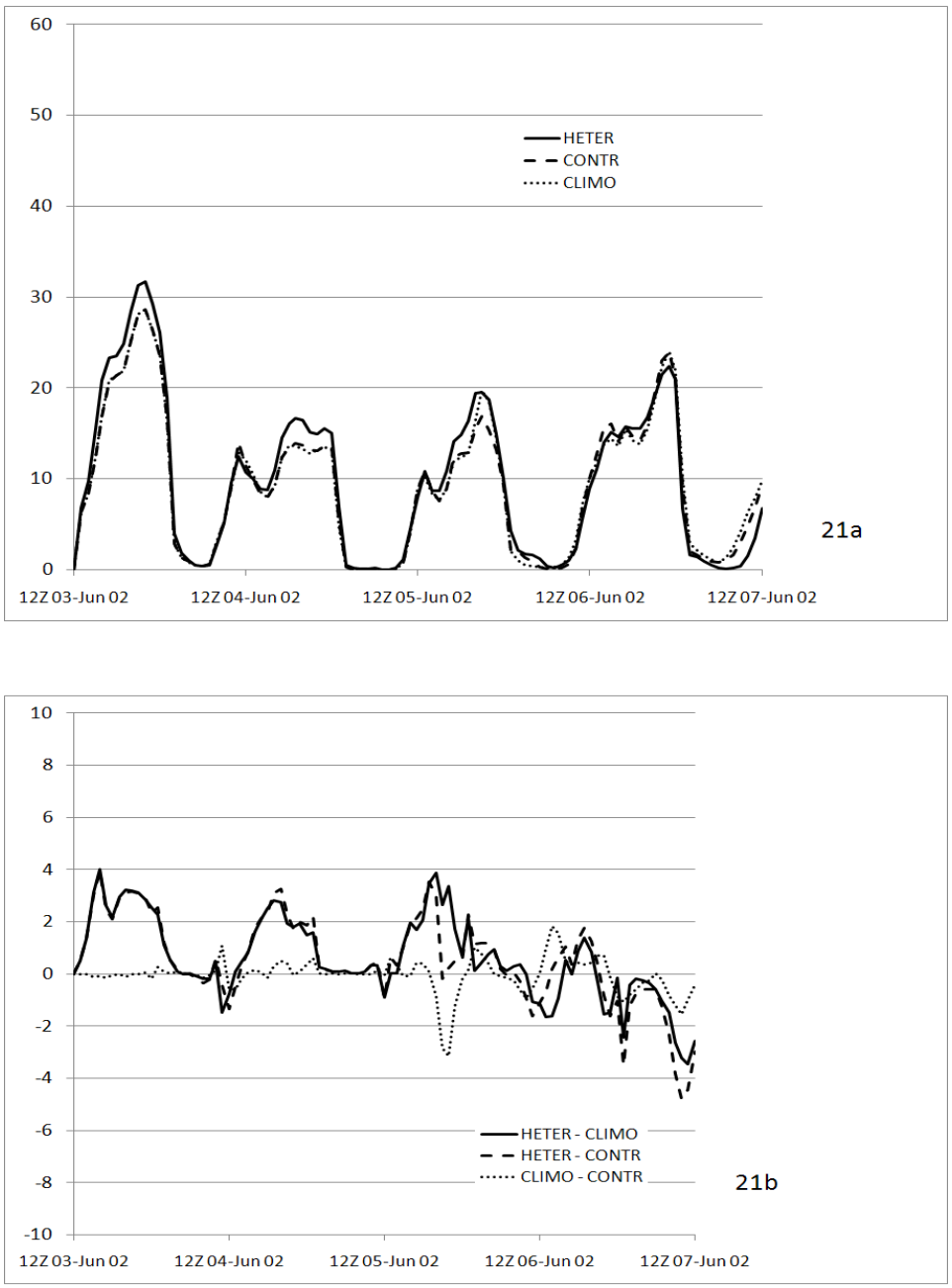

FIG. 21. MIXED domain averaged TKE (21a) and differences in TKE (21b) at 40m AGL over the 4 day integration. Results indicate that TKE is enhanced during mid-day by 10-20%.

Tables

TABLE 1. Comparison of mean z_0 values (meters) from various sources:

1. Brutsaert 1984; 2. Bonan et al. 2002; 3. Dorman and Sellers 1989; 4. Dickinson et al. 1993; 5. MODIS-based values over the study domain for June 3-7,2002.

Land Cover Type	**Field Expts**[1]	**CLM2**[2]	**NOAH**[3]	**BATS**[4]	**MODIS**[5]
Evergreen Needleleaf Forest	0.8-1.5	0.935	1.089	1.00	1.17
Evergreen Broadleaf Forest	1.5-2.5	1.925	2.653	2.00	1.34
Deciduous Needleleaf Forest	-	0.770	0.854	1.00	1.08
Deciduous Broadleaf Forest	0.4-0.7	1.100	0.826	0.80	0.54
Mixed Forest	-	1.100	0.563	0.80	0.65
Closed Shrubland	-	0.060	0.238	0.10	0.03
Open Shrubland	0.20-0.40	0.060	0.065	0.10	0.04
Grassland	0.008-0.06	0.060	0.035	0.06	0.06
Cropland	0.05-0.20	0.060	0.035	0.06	0.05
Bare Soil	-	0.000	0.011	0.02	N/A

TABLE 2. Roughness sublayer parameters for Raupach's model for five typical land cover types including evergreen needleleaf, deciduous broadleaf, grassland, croplands, and open shrublands. Parameters include form drag, C_R, maximum ratio of friction velocity to mean wind at canopy top $\left(\frac{u_*}{U_h}\right)_{\max}$, wake spreading coefficient, c, empirical coefficient α, and canopy area index at onset of skimming flow, Λ_{max}. Further explanation and application of these parameters are in Jasinski et al, 2005.

Land Cover Type	C_R	$\left(\frac{u_*}{U_h}\right)_{\max}$	c	α	Λ_{max}
Evergreen needleleaf	0.21	0.27	0.28	1.90	1.9
Decidous broadleaf	0.31	0.33	0.36	1.15	1.7
Grasslands	0.43	0.32	0.49	1.30	1.3
Croplands	0.31	0.29	0.39	1.60	1.5
Open Shrublands	0.50	0.38	0.48	1.00	1.6
Mean	0.35	0.32	0.40	1.40	1.6
Raupach 1994	0.30	0.30	0.37	N/A	0.6

TABLE 3a. MODIS Derived mean roughness length and standard deviation for each IGBP land cover type for June 3-7, 2002 for GRASS, MIXED and FULL domains shown in Figure 4. Land Cover Key: ENL, Evergreen Needleleaf Forest; EBL, Evergreen Broadleaf Forest; DBF, Deciduous Broadleaf Forest; MF, Mixed Forest; CS, Closed Shrubland; OS, Open Shrubland; WS, Woody Savanna; SV, Savanna; GR, Grassland; CR, Cropland; UR, Urban; CV, Cropland Vegetation Mosaic; W, Water.

	MODIS Derived									CONTR
Land Cover Type	GRASS			MIXED			FULL			All Cases
	%	z_0	σ_{z_0}	%	z_0	σ_{z_0}	%	z_0	σ_{z_0}	z_0 (σ_{z_0}=0)
ENL	0.03	1.19	0.21	9.98	1.16	0.14	1.81	1.17	0.16	0.94
EBL	0.01	2.92	N/A	5.40	1.30	0.87	1.17	1.34	0.90	1.93
DBF	0.00	N/A	N/A	14.7	0.61	0.59	7.75	0.54	0.56	1.10
MF	0.02	1.78	N/A	19.5	0.64	0.44	6.58	0.65	0.45	1.10
CS	0.11	0.04	<0.01	0.25	0.03	0.01	0.20	0.03	<0.01	0.06
OS	5.64	0.04	<0.01	0.27	0.03	0.01	3.92	0.04	<0.01	0.06
WS	1.85	1.35	0.07	22.4	0.90	0.28	14.6	0.95	0.30	0.86
SV	1.30	0.80	0.06	5.52	0.51	0.15	3.14	0.59	0.19	0.96
GR	61.5	0.07	<0.01	5.33	0.06	0.01	42.0	0.06	0.01	0.06
CR	11.2	0.04	0.01	6.49	0.05	0.01	8.75	0.05	0.01	0.06
UR	0.01	0.85	N/A	2.14	0.85	0.00	1.15	0.85	0.00	0.85
CV	18.8	0.05	<0.01	4.10	0.05	0.01	6.98	0.05	0.01	0.06
W	0.29	<0.01	<0.01	4.71	<0.01	0.00	1.73	<0.01	0.00	<0.01
Summary										
HETER	100	0.09	0.20	100	0.65	0.54	100	0.33	0.46	-
CLIMO	100	0.09	0.19	100	0.65	0.38	100	0.33	0.38	-
CONTR	100	0.09	0.15	100	0.85	0.44	100	0.40	0.47	-

TABLE 3b. MODIS Derived mean displacement height and standard deviation of displacement height for each IGBP land cover type for June 3-7, 2002 for GRASS, MIXED and FULL domains shown in Figure 4. Land Cover Key: See Table 3a.

	MODIS Derived									CONTR
Land Cover Type	GRASS			MIXED			FULL			All cases
	%	d_0	σ_{d_0}	%	d_0	σ_{d_0}	%	d_0	σ_{d_0}	d_0 (σ_{d_0}=0)
ENL	0.03	9.25	0.75	9.98	10.24	1.85	1.81	10.23	1.80	11.39
EBL	0.01	N/A	N/A	5.40	12.66	8.65	1.17	12.83	8.68	23.45
DBF	0.00	N/A	N/A	14.7	5.63	5.49	7.75	4.91	5.03	13.40
MF	0.02	N/A	N/A	19.5	6.21	4.42	6.58	6.28	4.44	13.40
CS	0.11	0.42	0.01	0.25	0.43	0.05	0.20	0.42	0.04	0.34
OS	5.64	0.34	0.02	0.27	0.35	0.04	3.92	0.34	0.02	0.34
WS	1.85	9.09	0.45	22.4	7.66	2.58	14.6	7.71	2.43	10.45
SV	1.30	4.45	0.28	5.52	3.93	1.28	3.14	3.96	1.10	5.42
GR	61.5	0.35	0.01	5.33	0.36	0.05	42.0	0.36	0.03	0.34
CR	11.2	0.25	0.02	6.49	0.28	0.04	8.75	0.27	0.03	0.34
UR	0.01	N/A	N/A	2.14	4.83	0.00	1.15	4.83	0.00	4.83
CV	18.8	0.27	0.01	4.10	0.28	0.07	6.98	0.27	0.05	0.34
W	0.29	<0.01	<0.01	4.71	<0.01	0.00	1.73	<0.01	0.00	<0.01
Summary										
HETER	100	0.55	1.29	100	5.85	5.10	100	2.65	3.99	-
CLIMO	100	0.55	1.29	100	5.85	3.36	100	2.65	3.29	-
CONTR	100	0.60	1.49	100	9.78	5.80	100	4.36	5.72	-

TABLE 4. Statistical summary for all times and all stations for the FULL domain. Bold underlines indicate the lowest value between the 3 integrations. There were roughly 250 stations per time interval for meteorological stations and 8 for the flux stations. Key: surface pressure (PSFC), 2m temperature (T2), dew point temperature (TD), wind speed (WPD), and in addition for the FULL domain, downward longwave (LWD), downward shortwave (SWD), sensible heat (H), and latent heat (LE). The HETER performed better than CLIMO or CONTR in 15 out of 24 statistics.

Statistic/Variable	HETER BIAS	HETER MAE	HETER RMSE	CLIMO BIAS	CLIMO MAE	CLIMO RMSE	CONTR BIAS	CONTR MAE	CONTR RMSE
PSFC (mb)	**0.40**	**1.28**	**1.96**	0.50	1.30	1.99	0.51	1.32	2.00
T2 (C)	**-1.05**	**2.78**	**3.69**	-1.59	2.96	3.96	-1.73	3.22	4.210
TD (C)	-0.86	1.89	2.38	-0.75	**1.76**	**2.24**	**-0.66**	1.78	2.25
WSPD (m/s)	1.30	1.91	2.35	**1.26**	1.89	2.32	**1.26**	**1.88**	**2.32**
LWD (W/m2)	0.28	**20**	**24**	-0.61	20.58	24.46	**0.07**	21.25	25.1
SWD (W/m2)	27.49	**91.29**	**110.49**	25.96	92.65	111.21	**21.42**	96.18	114.93
H (W/m2)	**45.53**	**72.17**	**85.96**	48.75	75.8	91.34	48.86	77.36	92.51
LH (W/m2)	-49.49	**84.16**	**97.84**	**-48.53**	84.51	98.12	-49.19	87.03	101.21

TABLE 5. Statistical summary for all times and all stations for the GRASS subdomain. Bold underlines indicate the lowest value among the 3 integrations. Roughly 10 observations per time interval. Either the HETER or CLIMO performed better than CONTR in all cases.

Variable	HETER BIAS	HETER MAE	HETER RMSE	CLIMO BIAS	CLIMO MAE	CLIMO RMSE	CONTR BIAS	CONTR MAE	CONTR RMSE
PSFC (mb)	**0.30**	**1.10**	**1.33**	0.37	1.11	1.34	0.36	1.11	1.35
T2 (C)	0.44	2.19	2.70	**0.19**	**2.08**	**2.56**	0.25	2.16	2.64
TD (C)	**0.09**	1.76	2.03	0.13	**1.68**	**1.97**	0.25	1.74	2.02
WSPD (m/s)	**0.69**	**1.64**	**2.01**	0.75	1.71	2.06	0.70	1.66	2.02

TABLE 6. Statistical summary for all times and stations for the MIXED subdomain. Bold underlines indicate the lowest value among the 3 cases. Both the HETER and CLIMO had more better statistics than CONTR. Roughly 3-5 observations per time interval.

Variable	HETER BIAS	HETER MAE	HETER RMSE	CLIMO BIAS	CLIMO MAE	CLIMO RMSE	CONTR BIAS	CONTR MAE	CONTR RMSE
PSFC (mb)	**0.52**	**1.08**	**1.25**	0.66	1.15	1.15	0.70	1.18	1.35
T2 (C)	**-3.87**	5.12	5.89	-4.19	**4.75**	**5.32**	-4.79	5.32	5.79
TD (C)	-2.64	2.83	2.98	-2.34	2.56	**2.73**	**-2.27**	**2.53**	2.74
WSPD (m/s)	0.89	1.71	1,97	**0.62**	**1.51**	**1.77**	0.65	1.57	1.83